Thesis Title: Design of Photonic Crystal Fiber based on 76+36 OAM modes for Fiber Communication

Course Code: CIS499

Semester: Fall 2023

Submitted By

Khalequzzaman Ansary

ID: 193-16-464

Department of Computing and Information System (CIS)

Daffodil International University

Supervised By

Mr. Md. Mehedi Hasan

Lecturer, Convener, Department of Computing and Information System (CIS)

Daffodil International University

Date of Submission: January 23, 2024

APPROVAL

This Project titled **"Design of Photonic Crystal Fiber based on 76+36 OAM modes for Fiber Communication"**, Submitted by **Khalequzzaman Ansary**, ID No: **193-16-464** to the Department of Computing & Information Systems, Daffodil International University has been accepted as satisfactory for the partial fulfillment of the requirements for the degree of B.Sc. in Computing & Information Systems and approved as to its style and contents. The presentation has been held on 23-01-2024.

BOARD OF EXAMINERS

Md Sarwar Hossain Mollah — **Chairman**
Associate Professor and Head
Department of Computing & Information Systems
Faculty of Science & Information Technology
Daffodil International University

Dr. Shekh Abdullah-Al-Musa Ahmed — **Internal Examiner**
Assistant Professor
Department of Computing & Information Systems
Faculty of Science & Information Technology
Daffodil International University

Md. Nasimul Kader — **Internal Examiner**
Assistant Professor
Department of Computing & Information Systems
Faculty of Science & Information Technology
Daffodil International University

Prof. Mohammad Shorif Uddin, — **External Examiner**
Professor
Department of Computer Science and Engineering
Jahangirnagar University

Declaration

I, **Khalequzzaman Ansary,** hereby declare that the work in this dissertation titled **"Design of Photonic Crystal Fiber based on OAM modes Supporting 76+36 OAM modes for Fiber Communication"** has been done by me under supervision of **Md. Mehedi Hassan,** Lecturer, Department of Computing and Information System (CIS) of Daffodil International University. I am also declaring that this project or any part of it has never been submitted anywhere else for the award of any educational degree like, B.Sc., M.Sc., Diploma or other qualifications.

Supervised By

23.01.2024

Md. Mehedi Hassan
Designation: Lecturer
Department of CIS
Daffodil International University

Submitted By

Khalequzzaman

Khalequzzaman Ansary
ID: 193-16-464
Department of CIS
Daffodil International University

Acknowledgement

I begin with sincere gratitude to Allah, the Most Merciful for granting me the strength, wisdom, and perseverance to complete my thesis, titled **"Design of Photonic Crystal Fiber based on OAM modes Supporting 76+36 OAM modes for Fiber Communication."**

First and foremost, I am deeply indebted to my honorable supervisor, **Md. Mehedi Hassan**, Lecturer in the Department of Computing and Information System (CIS) at Daffodil International University. His unwavering support, invaluable guidance, and insightful feedback were instrumental in shaping the trajectory of my research.

I extend my sincere thanks to the honorable head of the CIS department, **Mr. Sarwar Hossain Mollah**, for providing an enriching academic environment and facilitating with essential resources which was very encouraging for me from the beginning.

I am grateful to all the faculty members of the CIS department for their intellectual contributions and encouragement throughout my research work. Their encouragement and patience sustained me during the challenging phases of this academic endeavor.

This thesis work would not have been possible without the collaborative efforts and support of all those mentioned above. Thank you for being an integral part of my academic journey.

Dedication

I would like to dedicate this accomplishment to my beloved father **Anisur Rahman,** mother **Khairun Nahar,** whose unwavering love, encouragement and sacrifices have been my driving force behind my academic journey. Without their endless support and belief in my abilities, I would not have been able to pursue this opportunity to research or study in order to make a positive impact on society.

Abstract

This study introduces a innovative multi-layered photonic crystal fiber (PCF) featuring a pair of distinct and independent directed mode regions, collectively supporting a total of 112 orbital angular momentum (OAM) modes, comprising 76 + 36 modes. The designed nested PCF is characterized by a prominent primary channel, incorporating a pair of ring areas with high refractiveindex composed of Borosilicate glass (SF_6)*, surrounded by a cladding with fused silica as the background material. The findings indicate wherein the suggested PCF exhibits a adequately substantial effective refractive index difference (ERID), along with a consistently flat dispersion profile, expansive effective mode field area and minimal confinement loss across the wavelength range of 0.6 to 1* μm*. The confinement loss (CL) ranges approximately between* 2.49701×10^{-11} *to* $9.13425 \times 10^{-9}\ dB/m$*, while highest attained OAM purity is 99.31969% and 98.99258% at* $HE_{2,1}$ *mode respectively for both inner and outer rings. All the modes demonstrate ERIDs exceeding* 10^{-4} *, and minimum dispersion variation observed is* $-856\ ps/km-nm$*. Additionally, achieving an outstanding isolation performance, with the highest attained ISO reaching 294* dB *at* $HE_{9,1}$ *mode and observed a substantial effective mode area of 9.15* μm^2 *and 25.8* μm^2 *respectively for inner and outer rings. This research leverages COMSOL Multiphysics' finite element method (FEM) and perfectly matched layer (PML) capabilities alongside MATLAB processing to calculate all key variables of the offered fiber. Therefore, the suggested Photonic PCF demonstrates promising prospects for extended-range, high-capacity data transmission within optical communications and applications related to OAM sensing.*

Table of Contents

List of Figures

List of Tables

List of Abbreviations

PCF	Photonic Crystal Fiber
OAM	Orbital Angular Momentum
SDM	Space Division Multiplexing
MDM	Mode Division Multiplexing
LP	Linear Polarization
PML	Perfectly Matched Layer
FEM	Finite Element Method
S-PCF	Spiral Photonic Crystal Fiber
ERI	Effective Refractive Index
EMA	Effective Field Mode Area
ERID	Effective Refractive Index Difference
NA	Numerical Aperture
CL	Confinement Loss

List of Symbols

λ	:	Operating wavelength
c	:	Velocity of light in vacuum
l	:	Topological charge
C_{loss}	:	Confinement loss
η	:	Mode quality
ρ	:	Ratio of the annular radii of the ring
n_{eff}	:	Effective refractive index
D	:	Total dispersion
A_{eff}	:	Effective Area
n_2	:	Nonlinear coefficient
γ	:	Nonlinearity
Im	:	Imaginary part

Chapter 1

Introduction

1.1 Introduction

Photonic crystal fiber (PCF) is an innovative optical waveguide made with air-holes along its entire length. Proposed in 1996, PCF has become a well-established field in both research and commercial applications. Optical fibers derive their unique properties from a meticulously designed, highly transparent silica lattice, making them essential for advanced communication and data transmission. In recent years, engineers and scientists have focused on advancing optical fiber technology, particularly Photonic Crystal Fiber (PCF). Optical fiber is a slender, clear conduit that transmits large amounts of data over long distances using guided light in modern communication and data transfer systems. Optical fiber plays a crucial role in various fields, including medicine, sensing technologies, and laser applications, highlighting its versatile utility [1]. PCF, constructed with an artificial array of air holes along its length, outperforms standard optical fiber, offering superior performance [2]. PCF is an innovative optical fiber design which leverages the advantages of both optical fibers and photonic crystals, resulting in unique properties unattainable with traditional fibers. Unlike traditional optical fibers, Photonic Crystal Fiber (PCF) offers superior dispersion control, allowing for precise manipulation of light pulses. This capability is advantageous in applications such as high-speed data transmission where minimizing dispersion is crucial [3].

Moreover, PCF outperforms traditional solid-core fiber in terms of flexibility and bend sensitivity, allowing it to maintain superior guiding properties even under tight bends, making it ideal for applications where space constraints or intricate routing is required. Figure 1.1 illustrates the cross-sectional insight of the initial solid-core PCF [2], featuring a *300* nm perforation diameter and a pitch distance of *2.3* μm.

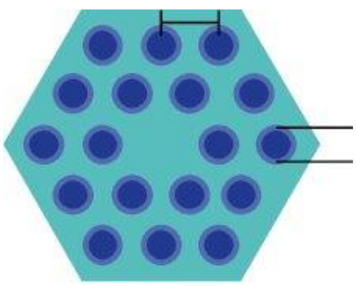

Figure 1. 1: Cross-sectional insight of first solid-core PCF.

Over three decades of dedicated research, continuous advancements in system capabilities and fabrication technology have approached their limits. Since the 1980s, researchers and engineers across multiple laboratories have been intrigued by the potential to structure materials at the optical wavelength scale (sub-micrometer dimensions) to create innovative optical mediums, commonly referred to as photonic crystals. Optical beam guidance relies on two primary mechanisms: total internal reflection (TIR) and photonic bandgap guidance (PBG). To facilitate TIR for guiding light, a cladding material featuring a refractive index sustain beneath that of the core is essential. However, no lossless materials with a refractive index beneath that of air at optical frequencies are currently available [1].

During 1998, the inaugural PCF utilizing the PBG influence for luminance guidance was documented [4, 5]. Hollow-core guidance became feasible in 1999 with advancements in PCF fabrication, allowing for higher air content proportions necessary to attain photonic bandgap with respect to aerial orientation. Hollow-core PCFs demonstrate significant potential due to their low nonlinearity [6] and high damage threshold [7-9]. This is attributed to the air-guiding in the hollow core, resulting in minimal overlap between silica and the propagating mode. Therefore, they emerge as favorable options for upcoming telecommunication transmission systems. Air-guiding PCFs hold potential for delivering high-power laser beams, applicable in areas like marking, machining, welding, laser surgery, and terahertz generation [10].

Optical fibers, while ideal for various applications, are presently impractical due to fiber damage, adverse nonlinear effects from high optical powers, and group-velocity dispersion causing short pulse dispersion [10]. Air-guiding photonic crystal fibers (PCFs) are ideal for nonlinear optical processes in gasses, with applications in trace gas detection and gas lasers. Losses are limited by factors like absorption, scattering, confinement loss, bend loss, and structural variations. Figure 1.2 illustrates the inner configuaration of the inaugular hollow-core PCF proposed in [3], featuring a pitch distance of $4.9\ \mu m$ and a core diameter of $14.8\ \mu m$.

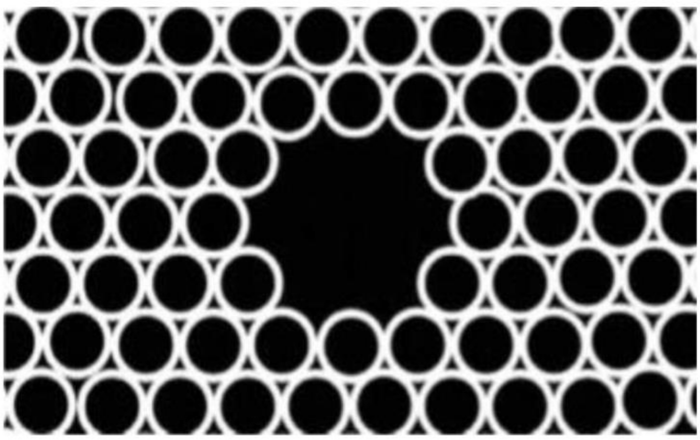

Figure 1.2: Inner configuaration of the inaugular hollow-core PCF

Circular PCF stands out as a unique optical light guide with a enchanced refractive index kernel (silica glass) and a encasement region formed by a ordered distribution of air apertures along the fiber [11]. Traditional fibers incorporate stringent composition constraints due to limitations in core size and material options. Light propagation relies on the total internal reflection (TIR) concept [12], leading to restricted distance coverage. Photonic Crystal Fibers (PCFs) are typically segregated into two types: index navigating and photonic band gap navigating. Each sort of PCFs allow for the manipulation of essential fiber properties for instance effective area [13], scattering [14], nonlinearity [5], dual refractivity [15], confinement loss, and transmission constant [6] through modification of aperture dimensions, spatial organization, and structure. The unique optical characteristics of PCFs have propelled their extensive applications in lightwave transmission [14, 16], nonlinear optics [5], and leading-edge technology [7].

The effective refractive index in PCF significantly impacts optical communication properties, serving as a vital parameter for system evaluation[13, 14]. Confinement loss in waveguides relies on the hypothetical segement of the effective refractive index [3] and effective area, while wavefront spreading and light transmission ratio are influenced by the legitimate section of the effective refractive index [13]. Refining the diameter and proposition of cladding perforations enables the design of application-specific guiding properties [9]. Space division multiplexing (SDM) is a promising solution for enhancing the potential of current lightwave transmission systems, as demonstrated in previous studies [17]. Extensive research and practical implementation have been conducted on SDM using both multimode fiber and multicore fiber, as documented in references [18-19]. In recent times, Orbital Angular Momentum (OAM) modular diversity is emerging as a optimistic evolution for space division multiplexing, enhancing transmission efficiency and bandwidth optimization [20]. Exploration of OAM signal trnamission has garnered considerable attention and undergone thorough investigation, as reflected in extensive studies [21-22].

To delve into the discussion on OAM, it is imperative to explore the principles of Spin Angular Momentum (SAM) and Orbital Angular Momentum (OAM). A beam exhibiting amplitude distribution described by $u(r, \phi, z) = u_0(r, z) exp(i\, l\phi)$, possesses angular momentum along the beam axis. The orbital contribution is exclusively influenced by the azimuthal phase dependence and is expressed per photon. Polarization dictates the spin angular momentum of material bodies. Each body can possess both spin and orbital angular momentum (OAM), with the OAM as a result of its linear motion. The total angular momentum for an assembly of components, represented by the inferior notation 'α', is possible to be defined as follows:

$$\boldsymbol{J} = \sum_{\alpha} \quad [(\boldsymbol{r}_{\alpha} \times \boldsymbol{p}_{\alpha}) + \boldsymbol{s}_{\alpha}] \qquad (1.1)$$

In this context, $\boldsymbol{r_\alpha}, \boldsymbol{p_\alpha}$ and $\boldsymbol{s_\alpha}$ represent the body $\alpha's$ position, linear momentum, and spin, respectively. The total spin $'S'$ and orbital angular momentum $'L'$ of a system can be determined by summing the individual quantities of each particle in the system:

$$S = \sum_\alpha s_\alpha \qquad (1.2)$$

$$L = \sum_\alpha r_a \times p_\alpha \qquad (1.3)$$

Spin and orbital angular momentum are typically correlated with intrinsic and extrinsic angular momentum, respectively. The displacement of the rotation axis origin can alter these values. Therefore, The external angular momentum J_{ext} is defined as the cross product between the center of mass position and the total linear momentum, P.

$$J_{ext} = R \times P \qquad (1.4)$$

Where,

$$R = \sum_\alpha \frac{m_\alpha}{M} r_\alpha;\ M = \sum_\alpha m_\alpha;\ P = \sum_\alpha P_\alpha \qquad (1.5)$$

The intrinsic angular momentum is the aggregation of spin angular momentum and orbital angular momentum with respect to the center of mass. The extrinsic angular momentum is influenced by changes in the velocity and displacement of rotation axes, while the intrinsic angular momentum remains unaffected by alterations in axis displacement. For a single body, orbital momentum aligns with extrinsic, and spin momentum corresponds to intrinsic. The external angular momentum component aligned with the total momentum is required to be zero. When analyzing a mechanical system with only a subset of bodies, the center of mass may vary from the overall system. The total angular momentum can be expressed easily in relation to the momentum density as follows:

$$J = \int \epsilon_0 r \times (E \times B) d^3x \qquad (1.6)$$

Enhancing transmission capacity remains a persistent and critical priority in optical fiber communications. The existing optical fiber communication systems are experiencing a bandwidth constraint at 100 terabits per second, marking the upper boundary within the C + L bands of unimode fiber [11]. Space division multiplexing (SDM) emerges as a core remedy to tackle the impending proficiency constraints. SDM implementation employs two main technologies: Multicore fibers, requiring complex fabrication for optimal core spacing, and Mode Division Multiplexing (MDM) using multimode fibers [2], which relies on spatial mode orthogonality to prevent crosstalk [12].

Two approaches are employed in the implementation of SDM:

1. Multicore fiber: Complex fiber fabrication is an essential requirement.

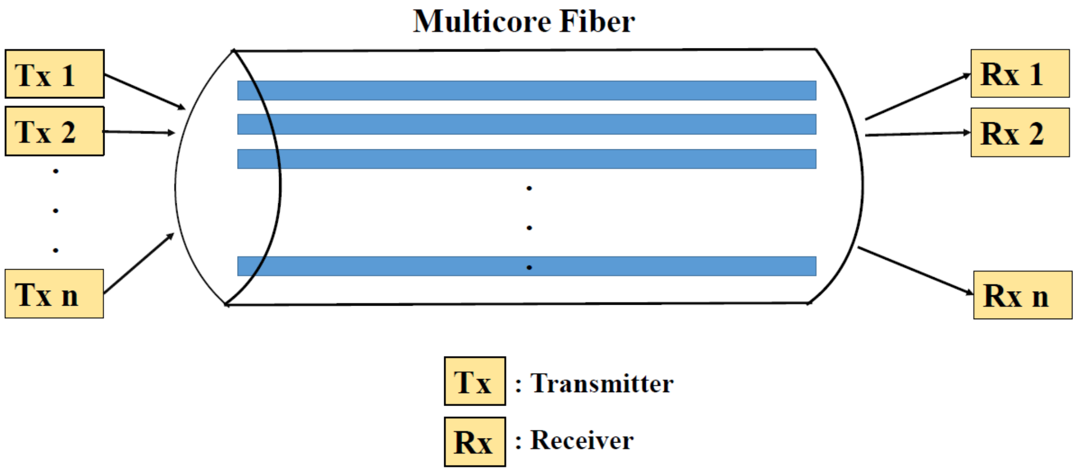

Figure 1.3: Utilization of multicore fiber in SDM implementation.

2. Mode division multiplexing (MDM): Utilizing the multimode concept.

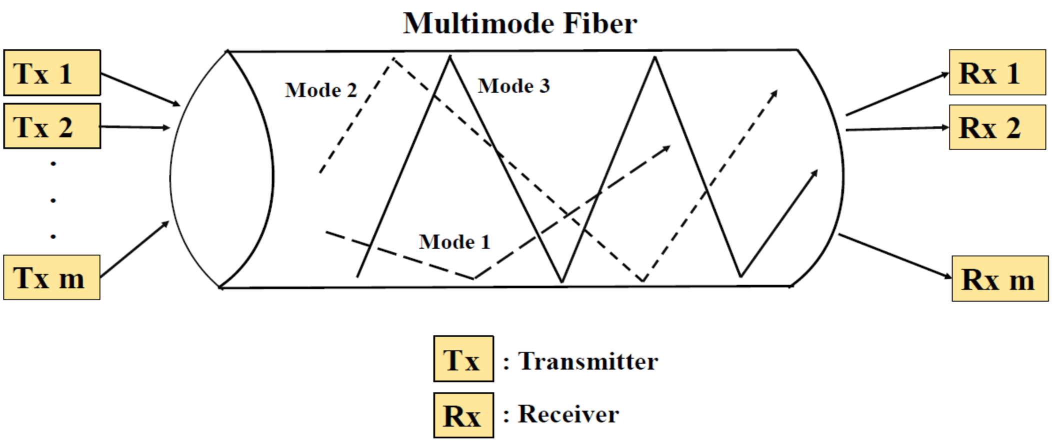

Figure 1.4: Utilization of multimode fiber in SDM implementation.

Two potential orthogonal modal basis sets for testing MDM systems are linearly polarized (LP) modes, consisting of vector modes with varying propagation constants, and OAM modes [3], fabricated with symmetric and asymmetric modes with nearly identical propagation constants within the same vector mode [4]. OAM modulates light by imparting a helical twist, expressed as $exp(il\varphi)$ [14], where $'l'$ signifies the helical torsion (mode), and $'\varphi'$ represents the angular orientation [23].

To prevent near-degeneracy in vector mode coupling to LP modes, the refractive index contrast between adjacent vector modes in this fiber should exceed 10^{-4}. Accordingly, this fiber type has two drawbacks: intricate manufacturing and increased transmission loss. Additionally, its moderately narrow ring core region results in a higher loss due to the rotational-electronic correlation impact. Employing PCF structures to support OAM modes is advantageous due to the enhanced design flexibility they offer. PCF enables the creation of unique fiber properties, including manageable nonlinearity, confinement loss, and tolerable spectrum scattering [24]. This approach enhances the adaptability and performance of optical communication systems. MDM fiber communications stand to benefit greatly from the application of PCF-based OAM modes.

Space Division Multiplexing (SDM) is a strategic technique that addresses and mitigates the constraints associated with fiber transmission capacity [9]. To achieve SDM, two approaches are examined: employing multicore technology and implementing mode division multiplexing in multimode fiber [25]. MDM systems can be explained in two ways: one utilizes a few mode fibers , while the other employs a greater number of mode fibers [26]. Orbital Angular Momentum (OAM) serves as a key element in spatial multiplexing within optics. The contemporary hurdle in information technology lies in enhancing the prowess and effectivenss of data transfer. In addressing the hurdle, SDM technique employs OAM for multiplexing. The inclusion of photon features lessens the strain on modern optical communication [27]. The first recognition of optics' OAM occurred in 1992, as Allen employed Lager Gaussian beams [28]. The OAM beam is denoted as $e^{il\phi}$, with $'l'$ representing waveguide index and $'\phi'$ as the angular orientation. Variable $'l'$ is a natural number encompassing both negative and positive values, including zero $(\ldots, -4, -3, -2, 0, +2, +3, +4, \ldots)$ [24].

Furthermore, different methods, like twisted fibers [9], spiral phase plates [29], cylindrical lenses, and helical lattice structures, are employed for OAM beam generation. Nowadays, twisted hollow-core fibers [30], spiral fibers [23], and various air-hole-based circular fiber structures are commonly employed for OAM mode transmission.

1.2 Motivation and Contribution

In recent years, the emphasis has been on crafting unique structures with accompanying OAM modes. Distinctive results were achieved to maximize OAM modes, minimizing confinement loss, maintaining flat dispersion, ensuring mode purity, and improving numerical aperture. The increased OAM mode count improves data encoding for seamless transmission and aids in the accurate detection of received information in relation to the transmitted data. Verification of transmitted data is achieved by examining mode properties on both transmission sides. OAM adaptation involves transmitter blending a conveyance signal alongside transmission pulse, utilizing the conveyance signal to carry OAM modal features and accentuating the importance of OAM mode in optical communication. Conventional optical fibers struggle with OAM configuaration transmission, leading to the development of a dedicated PCF for effective multimode support and enhanced fiber characteristics. Enhancing OAM mode diversity, Hu Zhang et al. recommended a ring-shaped PCF [31] featuring 10 states, and Nandam et al. introduced a spiral PCF featuring 14 supported modes [32]. Recent work by Xin Wan et al. involves the design of PCFs with modified cladding. These PCFs support 26 and 30 OAM modes, boast a $300\,nm$ bandwidth, and demonstrate low dispersion along with ultra-low confinement loss. Recent work by Xin Wan et al. [33] involves the design of PCFs with modified cladding. These PCFs support 26 and 30 OAM modes, boast a $300\,nm$ bandwidth, and demonstrate low dispersion along with minimal encasement drawback. Moreover, Wang et al. [27] developed a dual PCF covering a spectral range of $850\,nm$, featuring 26 OAM states. A circular-PCF, designed by ZI-ANG HU et al. [34], incorporates As_2A_3 cladding and supports 26 modes. The heightened refractive index of As_2A_3 adversely affects the OAM transmission process and its parameters. Xun Xu et al. [35] developed a circular four-ring hollow-core PCF supporting 30 OAM modes with a $900\,nm$ bandwidth. The article analyzes three PCFs, emphasizing the impact of structure and material.

In 2018, a study by Yu Lei et al. [35] presented a numerical analysis of a high refractive index (ri) OAM fiber with 76 supported OAM modes. In 2019, Yanan Kang et al. [36] from Shanghai University developed an air-core transmission fiber optimized for orbital angular momentum (OAM) transmission. The fiber was constructed using a step-index distribution, specifically engineered to support OAM modes characterized by the topological charge numbers $|\ell| = 1, 5, 6$, and 7. This innovative fiber design was demonstrated to effectively sustain these OAM modes within the wavelength range of $1530\,nm$ to $1565\,nm$. In contemporary research, the application of photonic crystal fiber (PCF) has become a promising method for multi-orbital angular momentum (OAM) modes transmission [37, 38]. PCF's unique cladding structure with air holes allows for increased control over light propagation, providing flexibility and specialized functionalities like dispersion management and nonlinear effects [39, 40].

According to [41], A ring fiber accommodating 36 OAM states was developed by Rush et al. in 2014. However, to achieve more significant refractive index contrasts, adjustments in the fiber's doping concentration using Complex Modified Chemical Vapor Deposition (MCVD) along with alternative aprroaches are required. Likewise, a dual guided mode micro-structured PCF has been engineered to support 30 OAM modes and 2 LP (Linearly Polarized) [3] modes in 2018 by Xu M et al. of South China Normal University [42]. To date, there have been no documented reports detailing the support of OAM modes within guided mode regions by PCF. However, the existing PCFs fall short for an effective fiber transmission infrastructure. Therefore, crafting an innovative PCF is crucial, enhancing OAM parameters for reliable transmission and broader application utility.

In chapter 3, an innovative multi-layered PCF featuring two distinct and independent directed mode areas, collectively supporting a total of 112 orbital angular momentum (OAM) modes, comprising 76 + 36 modes is fabricated and discussed. The designed nested PCF is characterized by a prominent core aperture, incorporating a pair of ring areas with high refractive index composed of Borosilicate glass (SF_6), surrounded by a cladding with fused silica as the foundational component. This PCF ensures low confinement loss ranging from 2.49701×10^{-11} to $9.13425 \times 10^{-9}\ dB/m$ and minimum dispersion variation observed is $-856\ ps/km - nm$. Additionally, highest attained OAM purity is *99.31969%* and *98.99258%* at $HE_{2,1}$ mode respectively for both inner and outer rings.

In chapter 4, the proposed PCF is proposed and analyzed based on the COMSOL Multiphysics' finite element method (FEM) and perfectly matched layer (PML) capabilities alongside MATLAB processing to calculate all key properties of the proposed fiber. All the necessary parameters are being examined over $400\ nm$ wavelength. In contrast to related research, the designed nested PCF showcases a relatively smaller core size. This chapter focuses on examining how core size, PCF size, air hole count and air hole arrangement influence the outcome. The lowest achieved confinement loss is 2.49701×10^{-11} while maintaining a higher ISO value of $294\ dB$ at $HE_{9,1}$ mode for the proposed PCF. The PCF is examined alongside other optical parameters in relation to OAM specifications.

1.3 Major Objectives

This thesis aims to achieve the following objectives:

- Designing unique PCF structure
- Investigating PCF design and performance analysis
- Optimizing OAM transmission capability in PCF
- Obtaining reduced confinement loss
- Investigating flattened dispersion fluctuations
- Achieving superior OAM purity
- Maximizing ISO effectiveness
- Sustaining a significant number of OAM modes

1.3 Thesis Outline

Using COMSOL Multiphysics, the proposed PCF is designed, simulated, and analyzed, leveraging its user-friendly interface for coexisting partial differential equation systems. COMSOL stands out as an essential tool in PCF design and simulation. In addressing the engineering and mathematical physics challenges, the finite element method (FEM) is applied. All optical fiber design simulations and analyses in this thesis are exclusively FEM-based. The application of FEM allows for the numerical solution of partial differential equations on specified tools, facilitating an accurate analysis of PCF features [43]. Time efficiency increases, and numerical precision is enhanced with FEM. The Perfectly Matched Layer (PML) and FEM jointly form a well-established simulation methodology for fiber design, analysis, and performance assessment. By merging optics, chemistry, mechanics, and acoustics, the FEM becomes a versatile tool, extensively applied in sectors like ship design, architectural planning, and vehicle simulation. The application of FEM extends to the analysis of microstructure fibers, allowing for precise evaluation of effective area, refractive index, loss, dispersion, and other parameters. Hence, FEM stands out as a formidable option for crafting PCF models.

Furthermore, MATLAB is used in this thesis to visualize data and perform numerical simulations. MATLAB serves as a key tool in the precise modeling of OAM in PCF systems. Its numerical simulation capabilities empower the implementation and resolution of mathematical models explaining light propagation in PCF, including the generation and manipulation of OAM. MATLAB's optimization tools contribute to the effective design and optimization of the PCF structure for OAM transmission efficiency. Facilitating electromagnetic field analysis, mode study, and data visualization, the software assists researchers in investigating OAM modes and their coupling in optical fibers. Moreover, MATLAB's programming versatility allows for the crafting of customized scripts and easy integration with various simulation tools, making it a comprehensive platform for OAM-based PCF modeling.

This thesis introduces a groundbreaking PCF structure that facilitates numerous OAM modes and versatile fabrication. Our analysis covers key optical communication metrics, including OAM mode count, purity, effective refractive index, differences in refractive index, dispersion variation, effective mode area, confinement loss, numerical aperture etc. Chapter 2 provides a comprehensive numerical analysis of key parameters. In Chapter 3, a novel PCF supporting 76+36 OAM modes was developed, showcasing ultra-low confinement loss and improved OAM purity. Chapter 4 provides a detailed performance evaluation of the engineered PCF.

2.1 Key features of the OAM mode transmission

2.1.1 Supported OAM modes

The optical communication system is affected by a variety of OAM modes. OAM modes in fibers are determined by combining odd and even modes of HE and EH, alongside normal modes of TE and TM. Hence, we can represent it through equations (2.1) and (2.2) [44]:

$$\left\{OAM^{\pm}_{\pm l,m} = HE^{even}_{l+1,m} \pm jHE^{odd}_{l+1,m} \;\; OAM^{\mp}_{\pm l,m} = EH^{even}_{l-1,m} \pm jEH^{odd}_{l-1,m}\right\}; \qquad (l > 1) \tag{2.1}$$

$$\left\{OAM^{\pm}_{\pm 1,m} = HE^{even}_{2,m} \pm jHE^{odd}_{2,m} \;\; OAM^{\mp}_{\pm 1,m} = TM_{0,m} \pm jTE_{0,m}\right\}; \qquad (l = 1) \tag{2.2}$$

In this notation, $'\pm'$ superscript indicates circular polarization (left or right), and $'\pm'$ subscript denotes spiral front rotation (left or right). $'l'$ signifies topological charge, $'j'$ demonstrates a $\pi/2$ phase shift, and $'EH'$ or $'HE'$ modes express a $\pi/2$ azimuthal rotation. $'m'$ is a constant radial index always set to one (1). The presence of 'accidental degeneracies' restricts OAM mode's support for $m > 1$, causing difficulties in multiplexing and demultiplexing [45]. Thus, we focus exclusively on low-order radial OAM modes $(m = 1)$.

2.1.2 OAM Purity

Multiple OAM modes supported in a fiber enhance mode purity and quality, leading to reliable transmission and diminished capacity requirements. Quality OAM modes are determined by the intensity of the light overlap factor, as outlined in equation (2.3) [46]:

$$\eta = \frac{I_r}{I_c} = \frac{\iint_{rings} |\vec{E}|^2 dxdy}{\iint_{cross-section} |\vec{E}|^2 dxdy} \tag{2.3}$$

In this context, $'I_r'$ signifies the average light intensity of the ring area housing all OAM modes, and $'I_c'$ stands for the average light intensity within the cross-section of the PCF structures. Moreover, equation (2.4) outlines the mathematical representation for the annular radii ratio in the ring region:

$$\rho = \frac{r_2}{r_3} \tag{2.4}$$

In ring-based PCFs, the inner and outer ring radii are designated as r_2 and r_3, correspondingly.

2.1.3 The Effective Refractive Index (ERI)

Effective Refractive Index (ERI) signifies the mode's refractive index as it propagates through the waveguide. The interrelation of operating frequency and effective refractive index is outlined through Sellmeier's empirical equation. To ascertain the refractive index of various materials using Sellmeier's equation (2.5) [47]:

$$n(\lambda) = \sqrt{1 + \sum_{i=1}^{m} \frac{A_i\lambda^2}{\lambda^2 - B_i}} \tag{2.5}$$

In this scenario, the Sellmeier coefficients m, A_i and B_i influence the refractive index's wavelength dependence, expressed as $n(\lambda)$. With varying background materials, Sellmeier coefficients fluctuate; for instance, employing fused silica yields $m = 3$ and Where $A_1 = 0.69616630$, $A_2 = 0.40794260$, $A_3 = 0.89747940$, $B_2 = 0.00467914826$,$B_2 = 0.0135120631$, $B_3 = 97.9340025\ \mu m^2$. Alterations in the effective refractive index affect optical parameters, including dispersion profile.

2.1.4 The Effective Refractive Index Difference (ERID)

ERIDs assess sheer variations amidst HE and EH OAM states, with a defined threshold of 10^{-4} based on equation (2.6) [46]:

$$\Delta n_{eff} = \left| n_{eff_{HE_{l+1,m}}} - n_{eff_{EH_{l-1,m}}} \right| > 10^{-4} \tag{2.6}$$

ERID is a dimensionless parameter and indicated by its symbol Δn_{eff}. Coupling of OAM modes (HE and EH) takes place if differences are below 10^-4, moving towards linear polarization (LP). Balancing LP modes with component vector modes demands preserving the distinct propagation of each OAM mode and minimizing inter-mode crosstalk. Optimizing ERID reduces OAM transmission crosstalk, enhancing the quality of fiber communication [47].

2.1.5 Chromatic Dispersion

Dispersion emerges as a critical parameter in PCFs, influencing optical fiber transmission. Its adverse effects constrain efficiency improvement of spatial gap and signal propagation speed. The combined impact of waveguide and material dispersion constitutes the gross dispersion of fibers. At transmitting time, dispersion results in the enlargement of the light pulse. Furthermore, it encompasses waveguide and material dispersion [13]. The calculation excludes material dispersion due to its small impact on overall dispersion. Thus, the calculation is exclusively focused on waveguide dispersion, as outlined in equation (2.7) [48]:

$$D = D_m + D_w = -\frac{\lambda}{c}\frac{d^2 n[\lambda]}{d\lambda^2} - \frac{\lambda}{c}\frac{d^2 Re[n_{eff}]}{d\lambda^2} \qquad (2.7)$$

In this equation, D_w and D_m denote waveguide and material dispersion, respectively, with symbols λ and c. Here, λ represents wavelength, and c signifies the luminous velocity in a vacuum ($3 \times 10^8\ ms^{-1}$). The authentic portion of the Effective Refractive Index (ERI) is expressed as $Re\ [n_{eff}]$.

2.1.6 Effective Mode Area

Optical accpetance ratio and nonlinearity features show an opposite interrelation with alterations in the effective mode area. Determined through the equation (2.8), it is identified by A_{eff} [49].

$$A_{eff} = \frac{\left(\iint |E(x,y)|^2 dxdy\right)^2}{\iint |E(x,y)|^4 dxdy} \qquad (2.8)$$

Within the transverse electromagnetic field, $E(x, y)$ characterizes the lateral electric field distribution, and the double integral accounts for the entire cross-section of the PCF. A strong correlation exists between A_{eff} size, effective index difference, and core diameter [42]. However, for single-mode operation in radial multi-mode fibers, a large core area proves counterproductive, leading to heightened branching crosstalk [50].

2.1.7 Numerical Aperture

Numerical Aperture (NA) is a measure of the optical fiber's capacity to gather all the light rays or optical power within the fiber. NA holds paramount significance in diverse operative uses. A heightened NA improves lateral resolution but reduces depth of field (DOF), while a lower NA increases depth of field but diminishes lateral resolution [51]. It is a fundamental unitless parameter of optical fiber, and is determined by the expression provided in the equation (2.9) [46]:

$$NA = \left[1 + \frac{\pi A_{eff}}{\lambda^2}\right]^{-\frac{1}{2}} \qquad (2.9)$$

Where A_{eff} and λ represent the effective area and operating wavelength of the described PCFs.

2.1.8 Confinement Loss

Confinement loss PCFs arise from structural designs leading to light leakage through the cladding, causing immediate transmission distance collapse due to imperfect internal structure and the finite number of air-holes and layers [53]. A high CL negatively affects the generation of OAM modes by causing signal degeneration in the corresponding channel. To mitigate this issue, it is crucial to minimize CL, as it is identified as a harmful parameter in the process. Due to this fact, a lower CL enhances the efficient propagation of OAM states with minimal fiber attenuation. CL is assessed employing the refractive index's hypothetical value, determined mathematically through the equation (2.10) [52]:

$$C_{loss} = \frac{2\pi}{\lambda} \frac{20}{\ln\ln(10)} 10^6 \, Im(n_{eff}) \, (dB/m) \qquad (2.10)$$

Where, the controlling wavelength is denoted by $'\lambda'$, and $'Im(n_{eff})'$ represents the imaginary part (Refractive Index).

2.1.9 Isolation (ISO) Parameters

The extent of power leakage between the ring and core guided channels is assessed through the isolation parameter (ISO). To assess isolation effects and inter-core crosstalk, the ISO provides a valuable calculation method [54]. $(ISO_{r \to c})$ and $(ISO_{c \to r})$ are designated ISO parameters specifically designed to measure crosstalk power from core to ring and vice versa. The degree of power leakage into the ring region is captured by $ISO_{c \to r}$, whereas $ISO_{r \to c}$ captures the leakage into the core region. The determination of the ISO follows the procedures detailed in equations (2.11) and (2.12) [55]:

$$ISO_{O \to I} = -10 \times log \frac{\iint_{Inner}(E_x H_y - E_y H_x)dxdy}{\iint_{total}(E_x H_y - E_y H_x)dxdy} \quad (2.11)$$

$$ISO_{I \to O} = -10 \times log \frac{\iint_{Outer}(E_x H_y - E_y H_x)dxdy}{\iint_{total}(E_x H_y - E_y H_x)dxdy} \quad (2.12)$$

With E_x, E_y, H_x, and H_y denoting the electro-magnetic elemental factors of the respective states.

Design and Investigation of the Proposed PCF

3.1 Design Model and Methodology

Employing COMSOL Multiphysics 4.4 software, we designed and simulated the proposed dual guided nested PCF, characterized by H-shaped air holes in the outer layer. Consequently, MATLAB was applied for visualizing the results of the simulation. The proposed model features a core with a radius of *1.40* μm. The perforations of the nodal ring are circular shaped and marginal layer is featured by eight H-shaped circular ai-holes.

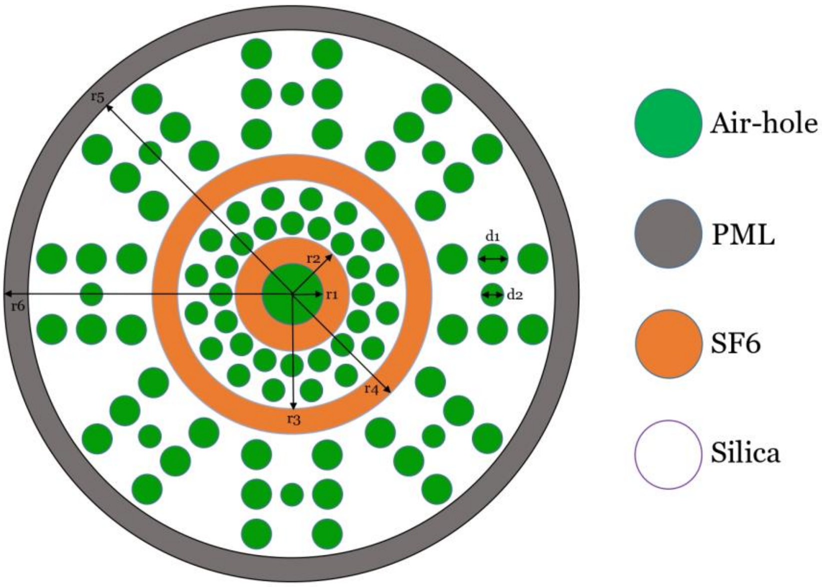

Figure 3.1: Cross-sectional insights of multi-layered PCF.

The cross-sectional representation in Figure 3.1 illustrates the meticulous construction of the multi-layered PCF. This particular PCF was tailored to accomodate the transmission speed OAM states, achieved via incorporating two distinct guided mode regions. Notably, the outer layer is characterized by H-shaped air holes. In order to meet the requirement for a low nonlinear coefficient, it becomes essential to carefully pick a substance with a moderate nonlinear index. Hence, the nested PCF is meticulously crafted on a silica substrate, possessing a refractive index (n) of 1.444 at 1.55 μm. Figure 3.1 presents a visual representation wherein different materials inside the Photonic Crystal Fiber (PCF) are distinguished by unique colors. The study incorporates ring structures characterized by inner and outer radii, denoted as r_1, r_2, r_3, and r_4. The associated parameters are specified as follows: $r_1 = 1.40\ \mu m$, $r_2 = 2.60\ \mu m$, $r_3 = 5.2\ \mu m$, $r_4 = 6.40\ \mu m$, as outlined in Table 1.

Table 1: Description of designed multi-layered PCF

Attributes	r_1	r_2	r_3	r_4	r_5	r_6	d_1	d_2
Description	Radius of the core	Radius of the nodal ring	Nodal radius of marginal ring	Marginal radius of marginal ring	Nodal radius of PML	Marginal radius of PML	Diameter 1	Diameter 2
Value (µm)	1.40	2.60	5.2	6.4	12.1	13.15	1.35	1.00

The findings presented here conduct a detailed investigation into nested Photonic Crystal Fiber (PCF), concentrating on essential parameters like supported modes, dispersion features, and non-linear coefficients. Employing two concentric ring structures, guide mode regions are precisely delineated, and strategic placement of air hole layers between them ensures effective separation. The outer layer features eight strategically incorporated H-shaped air holes, influencing the attributes of transmitted modes within the outer ring structure. The arrangement of perforations is crucial in determining the air filling fraction, with higher values proving advantageous in mitigating the observed confinement loss in the PCF. As a result, the inner layer integrates a total of 32 air holes, denoted as N_1, with their corresponding diameters identified as d_1 and d_2. Within the cladding arrangement, the nested PCF design showcases eight H-shaped air holes in each layer, where each H-shaped pattern encompasses seven air holes. Hence, the outer layer is characterized by a combined count of 56 air holes, labeled as N_2. The specified measurements for each layer in the configured PCF are presented as follows: $d1 = 1.35\ \mu m$, with $d2 = 1.00\ \mu m$. A thorough investigation of the designed nested Photonic Crystal Fiber (PCF) was conducted using the full-vector FEM. To improve the accuracy of the analysis, a PML was incorporated, leading to reliable insights into the fiber's light propagation behavior.

In PCF simulations, each wavelength exhibits four OAM modes—two HE (Hybrid Electric) modes and two EH (Electric Hybrid) modes, encompassing both even and odd modes within each category which has been shown in Fig. 3.2.

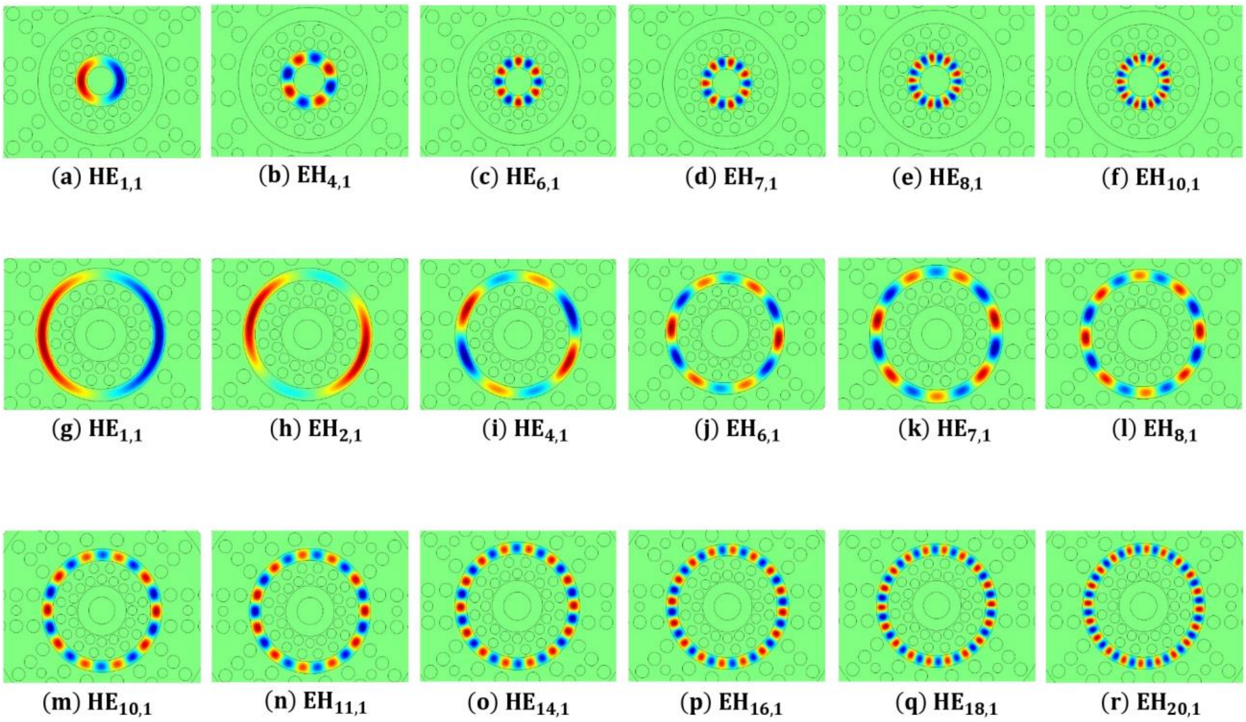

Figure 3.2: Electric Field Intensity.

The field distributions, characterized by intensity and phase variations, for discrete OAM and Linearly Polarized (LP) beams within the provided PCF are illustrated in Figure 3.2. The field distributions, characterized by intensity and phase variations, for discrete OAM and Linearly Polarized (LP) beams within the provided PCF are illustrated in Figure 3.2.

A comprehensive analysis establishes that the proposed PCF successfully accommodates all specified modes within the $0.6\,\mu m - 1.0\,\mu m$ wavelength range. Simulations leveraging these modes offer crucial validation for the suggested design. Having a greater quantity of OAM states is a key for better quality OAM-based PCF. Therefore, the proposed nested PCF is able to support a large number of OAM modes totalling 112 OAM modes, comprising 76 + 36 OAM modes.

3.2 Results and Discussions

The suggested PCF is designed to handle a total of 112 modes, comprising 76 + 36 OAM modes effectively, minimizing confinement loss, maintaining flat dispersion and featuring a minimal light gathering index alongside ensuring a refractive contrast above 10^{-4} amidst couple of neighbouring OAM states. Moving on, let's explore the characteristics of OAM covering the basics, like how light moves and changes. We'll get into details about optimal refractive index, dispersion, waveguide region, light gathering ratio and encasement deficit, explaining each featuring equations anlongside visuals.

Effective Refractive Index (ERI):

ERI significantly influences optical attributes, including dispersion variation, nonlinear behavior, and other relevant variables. Optical features, such as how light spreads and behaves uniquely, can be notably influenced by the ERI.

(a)

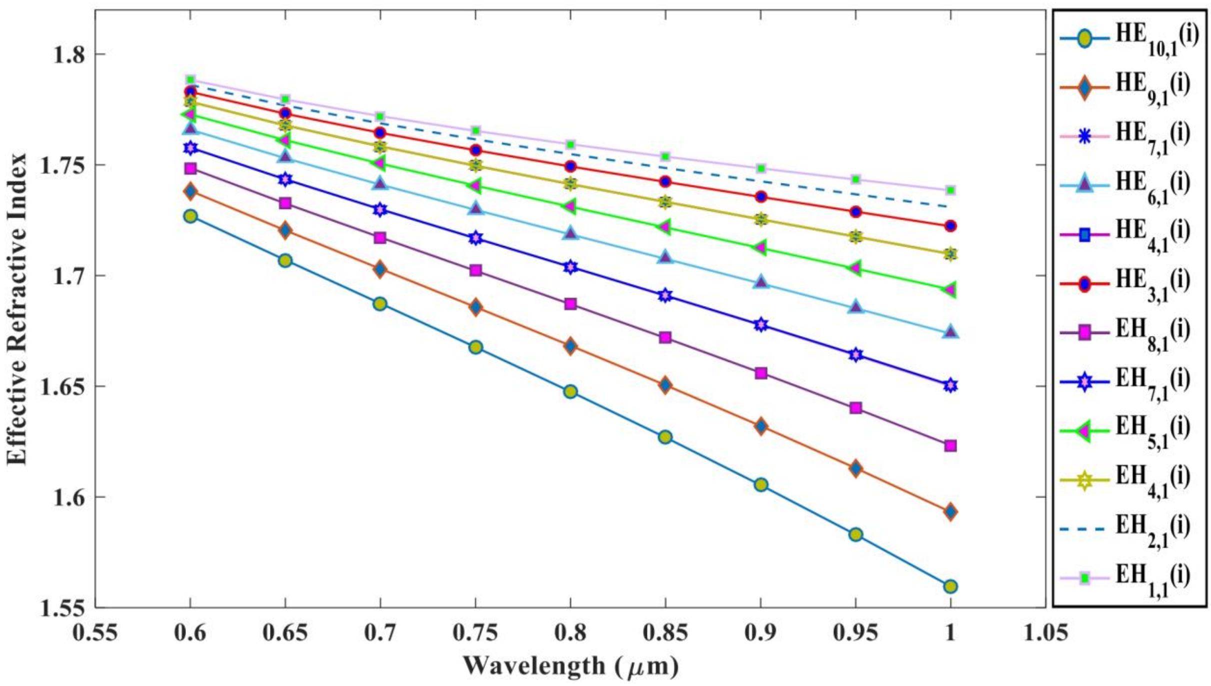

(b)

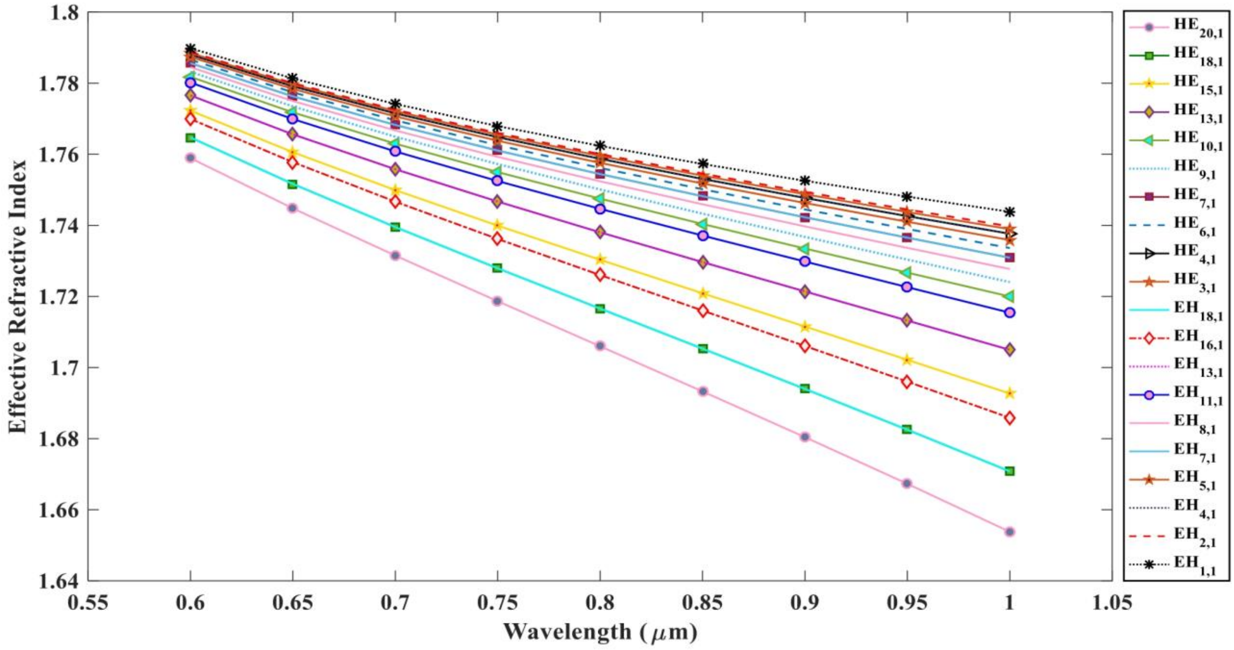

Figure 3.3: ERI of (a) nodal ring supported modes. (b) marginal ring supported modes.

Figure 3.3 (a) and (b) presents the wavelength-dependent effective refractive index (ERI) of diverse OAM modes in the designed nested PCF. Fused silica and sulfur hexafluoride (SF_6) are employed as the background and ring-core channel materials, respectively, within the structured design of the nested PCF [Fig. 3.1]. Hence, the mathematical assessment of the ERI for these materials is conducted through the application of the Sellmeier equation (2.5). The observed data indicates an inverse correlation between ERI and wavelength. Fig. 5. also reveals that EH vector modes exhibit higher ERI than HE vector modes in the proposed PCF across different wavelengths. The simulation reveals that lower-order OAM modes indicate higher frequency through wavelength variation. The outer ring layer exhibits a higher ERI in comparison to the modes supported by the inner ring layer. For example - ERI of $EH_{2,1}$ is *1.75486* and *1.76003* for inner and outer ring layers correspondingly.

Chromatic Dispersion:

Dispersion parameter plays a major role in how PCF operates. Increased dispersion adversely affects PCF performance. The fiber's rapid signal propagation is guaranteed by its flat and low dispersion properties.

(a)

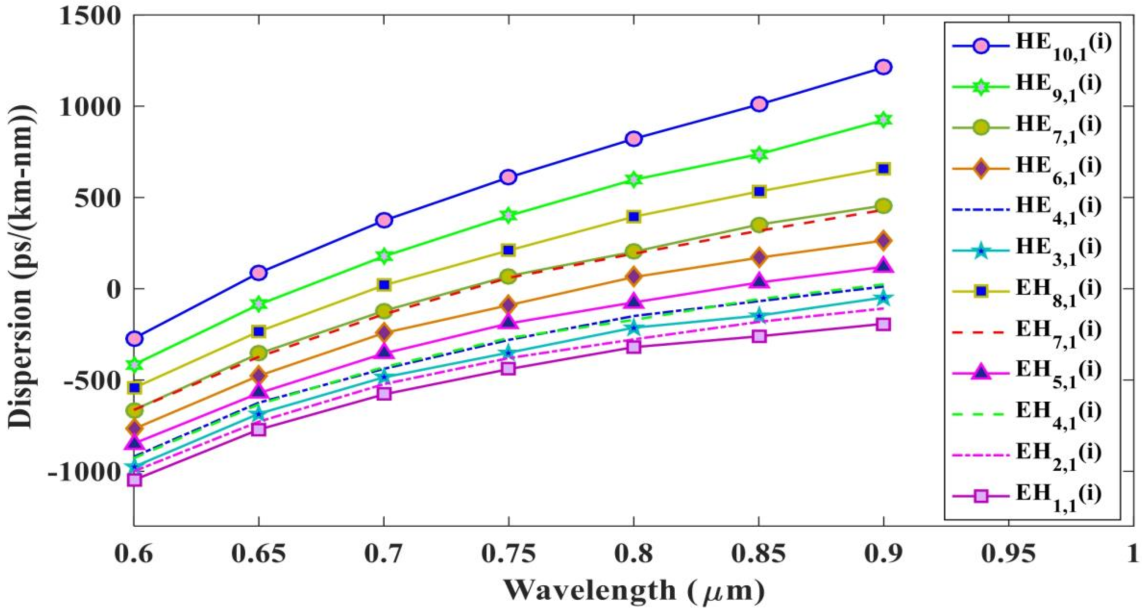

(b)

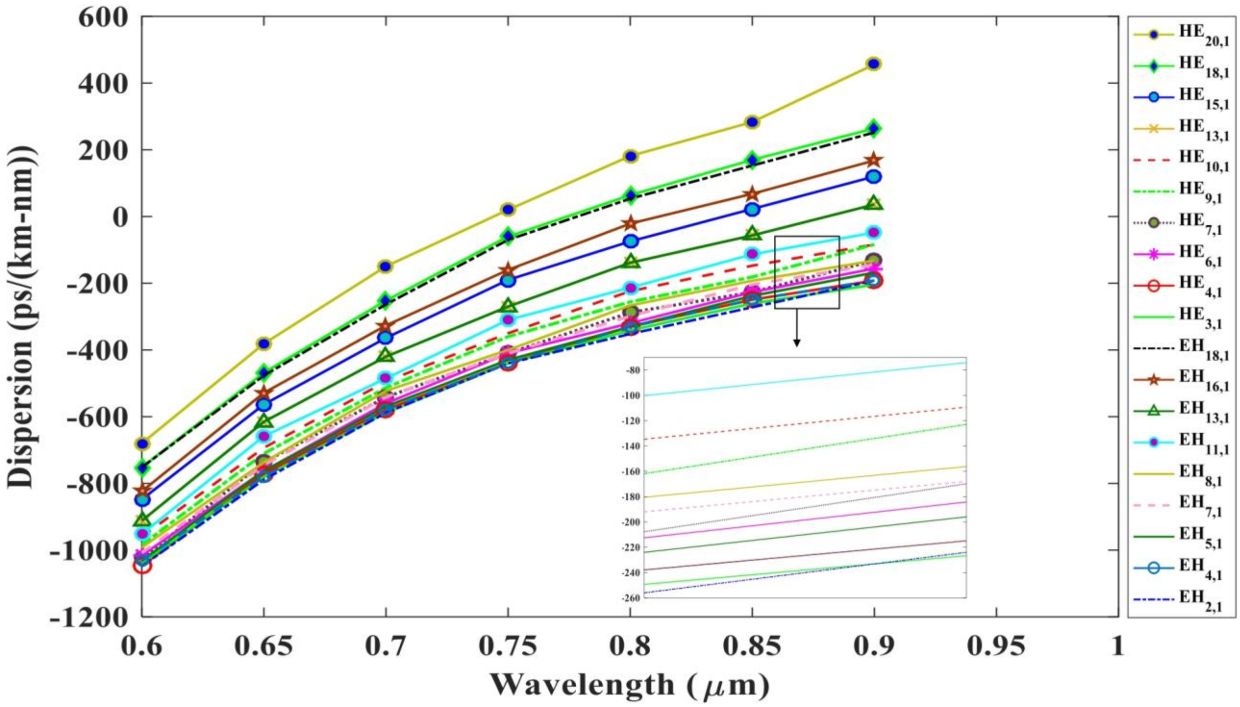

Figure 3.4: Wavelength-dependent dispersion characteristics of (a) modes supported by nodal ring, (b) modes supported by marginal ring.

The proposed fiber's dispersion profile can be mathematically expressed by equation (2.7), representing the total dispersion. Although both material and waveguide dispersion contribute to the total dispersion, the latter emerges as the primary driver in the designed nested PCF. Scattering features of the PCF under consideration are visually depicted in Fig. 3.4 (a) and (b). The nested PCF shows a higher dispersion of light with longer wavelengths in both its inner and outer rings. The EH mode exhibits lower dispersion than the HE mode due to its larger refractive index at the same order. For example - At $850\ nm$ wavelength, the dispersion value of $EH_{7,1}$ mode (inner ring) is $317.3333\ ps/km-nm$, while the dispersion observed at $HE_{7,1}$ mode is $351.3333\ ps/km-nm$. The dispersion trend is low and flattened for lower-order OAM modes, whereas higher-order OAM modes exhibit significant variation. Upon examining Fig. 3.4, it is observed that the lowest dispersion variation for both inner and outer ring is $-856\ ps/km-nm$ at $EH_{1,1}$ and $EH_{2,1}$mode respectively.

Effective Refractive Index Difference (ERID) of OAM Modes:

ERID simulations for multiple OAM states are depicted in Fig. 3.5.

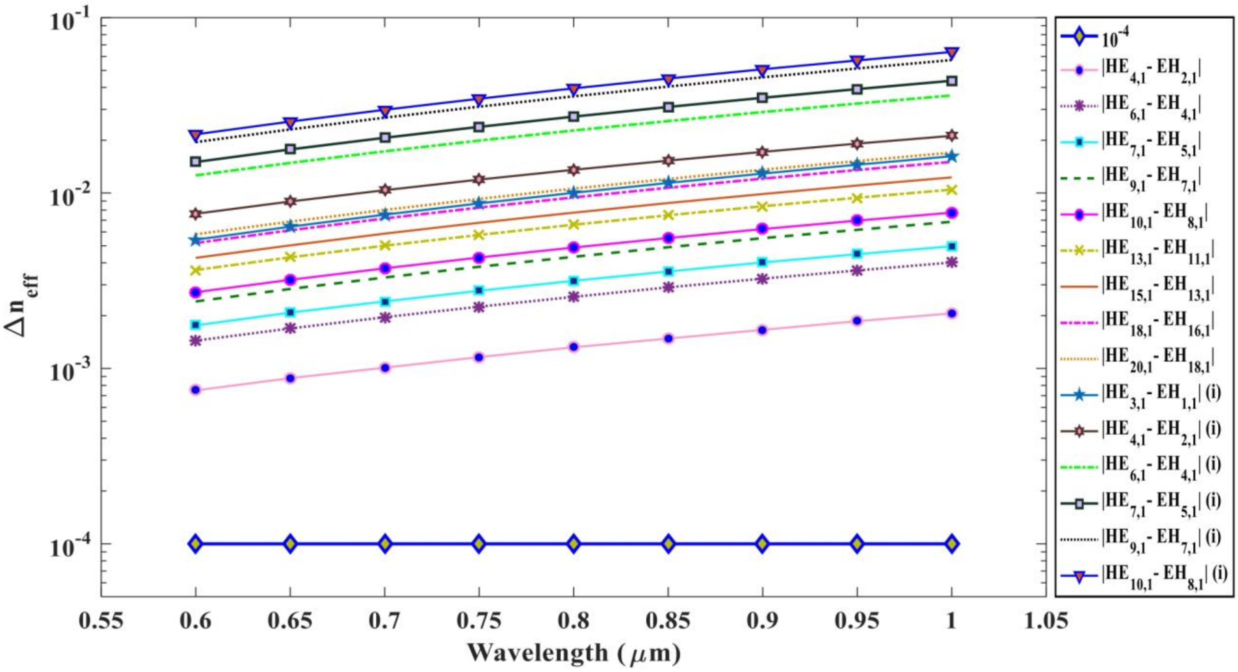

Figure 3.5: The ERID of several OAM states versus operating frequency.

Maintaining a Δn_{eff} value above 10^{-4} is essential to uphold a significant contrast between air-cladding and core materials, thereby preventing crosstalk among the channels. In this figure, the blue line represents 10^{-4}, and the results indicate that all ERIDs exceed this value. Upon examining Fig. 3.5, it is observed that there is a notable increase in the effective refractive index (Δn_{eff}) as the wavelengths are extended. Therefore, it can be concluded that the Effective Refractive Index Difference (Δneff) is correlated with the wavelength.

The Effective Mode Area (EMA):

EMA significantly influences OAM mode transmission, while changes in the numerical aperture feature distinctly affect the effective area (EA). The effective mode area of various supported OAM vector states are portrayed in Figure 3.6 (a) and (b) versus operating frequency.

(a)

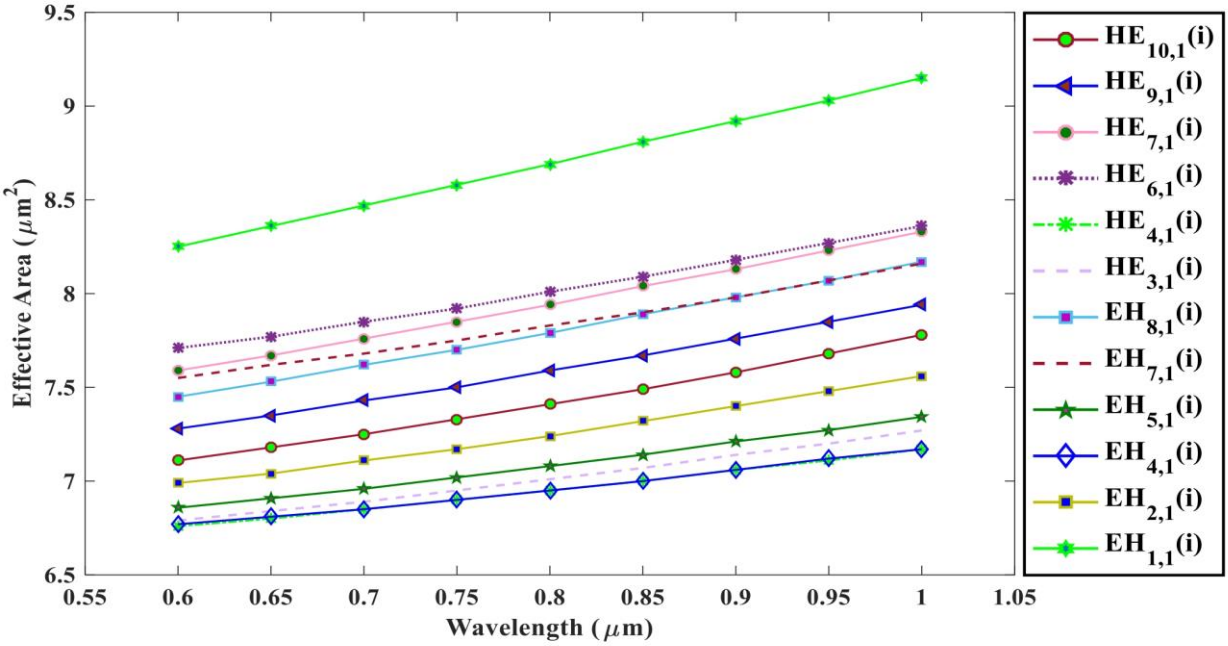

(b)

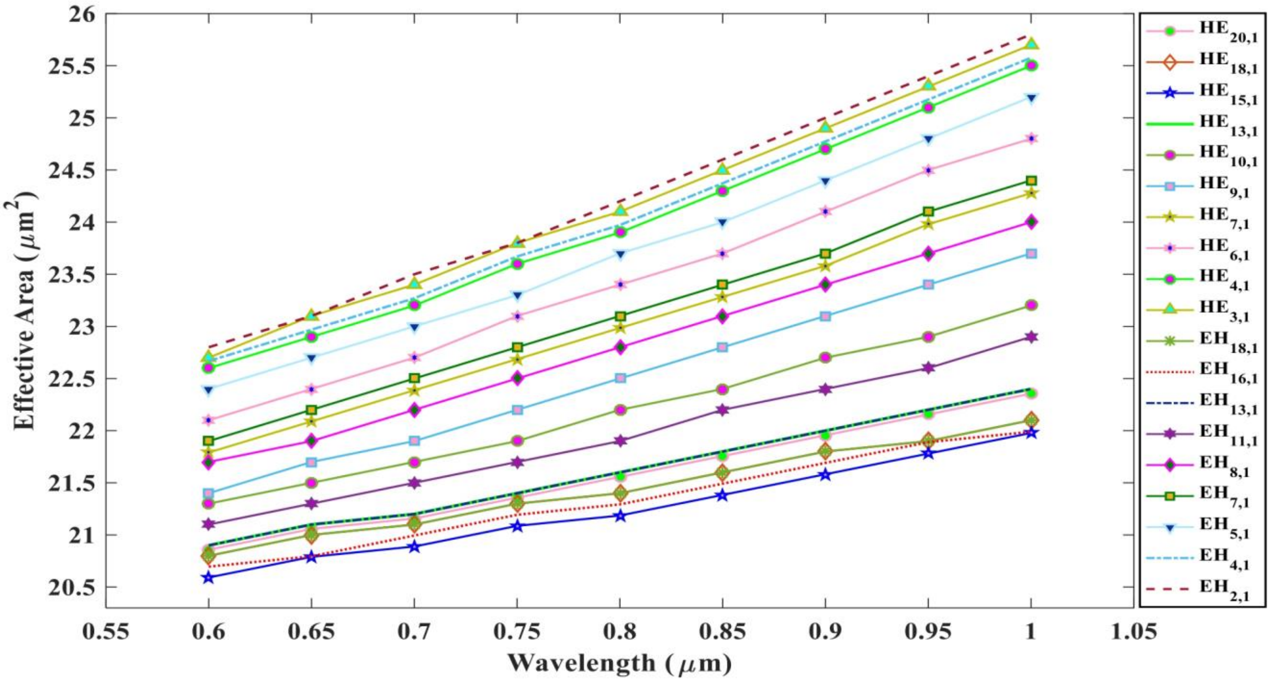

Figure 3.6: Wavelength-dependent EMA of (a) modes supported by inner ring (b) modes supported by outer ring.

The effective area of the nodal ring-supported mode varies from *6.76* to *9.15* μm^2, while for the marginal ring-supported mode, it varies between *20.6* and *25.8* μm^2. Upon an in-depth analysis of Fig. 3.6, it becomes evident that the Higher-order OAM modes illustrate a reduced effective field area due to an augmented light intensity leakage into the cladding region. Conversely, lower-order vector modes exhibit a moderate increase in the mode-field area. The challenge lies in restricting OAM at broader wavelengths, especially for higher-order modes prone to cladding leakage. Nevertheless, an extensive area does not facilitate the reduction of crosstalk in fiber optics by minimizing branching. Our proposed nested PCF addresses this challenge by minimizing crosstalk among branches through maintaining a narrow range of effective mode field region.

Numerical Aperture (NA):

The Numerical Aperture (NA) characterizes the optical fiber's ability to collect the total luminous wave within PCF. It is a fundamental unitless parameter of fiber. Optical field utilizes increased NA standards for various applications, and lower NA values play a role in expanding depth of field (DOF). According to Equation (2.9), it is evident that the effective area decreases as the Numerical Aperture (NA) increases.

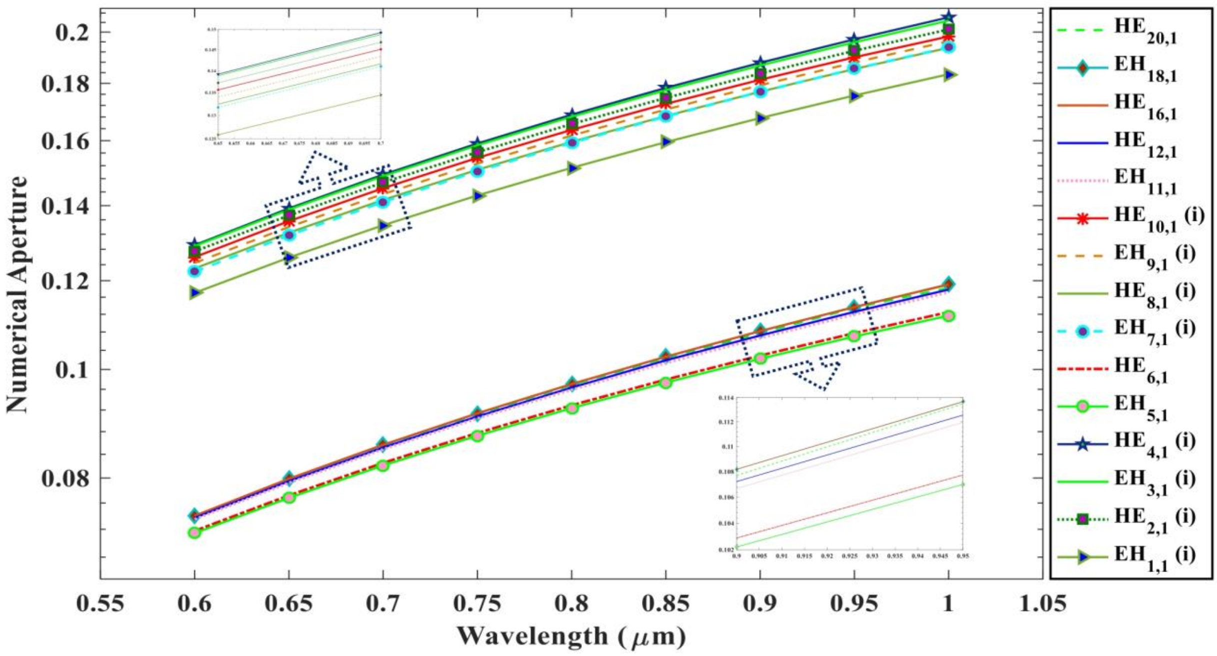

Figure 3.7: Wavelength-Dependent Numerical Aperture Analysis of Isolated Vector Modes

Figure 3.7 illustrates a positive correlation between the numerical aperture (NA) and wavelength in the proposed model. Increasing the order of OAM modes from *0.6* μm to *1.0* μm wavelength results in a polite rise in numerical aperture (NA), reaching its maximum where the effective area is minimized [Fig. 3.7]. For example - The proposed nested PCF achieves its highest $NA = 0.206154837$ for the $HE_{4,1}$(inner) mode where the effective mode area is minimum, making it particularly valuable in medical imaging, optical coherence tomography (OCT), and sensing applications.

Confinement Loss (CL):

Figure 3.8 clearly depicts the confinement loss of partially accomodated states in suggested multi-layered PCF. The CL of the specified vector modes in Figure 3.8 doesn't follow a linear trend with wavelength, unlike other optical parameters due to a higher chance of leakage towards the cladding.

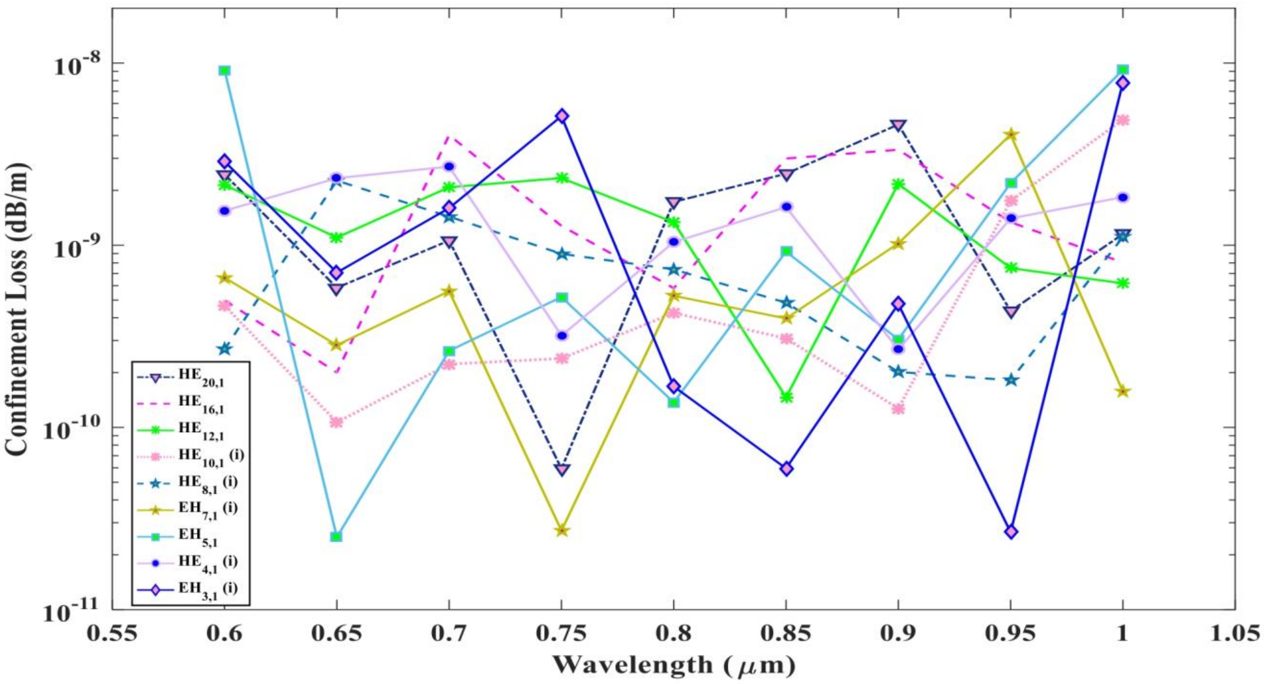

Figure 3.8: Confinement loss of some supported states against operating frequency.

Observed fluctuating trend in CL for both inner and outer rings, ranging approximately between 2.49701×10^{-11} to $9.13425 \times 10^{-9}\ dB/m$ orders of magnitude, suggests that the designed structure maintains a consistently low level of confinement loss. Specifically, the $EH_{5,1}$ (outer) mode at a wavelength of $650\ nm$ exhibits the minimum confinement loss of $2.49701 \times 10^{-11}\ dB/m$ because it possesses the lowest imaginary part of the refractive index within the nested PCF. The low confinement loss makes the structure ideal for stable OAM transmission and a promising choice for fiber communication applications.

OAM Purity:

The purity of specific OAM modes of both inner and outer rings is analyzed at the $0.8\ \mu m$ wavelength, chosen for its minimal confinement loss (CL), and depicted in Figure 3.9 The research findings suggest that, for the same OAM mode sequence, the purity of the HE state is larger than that of the EH state.

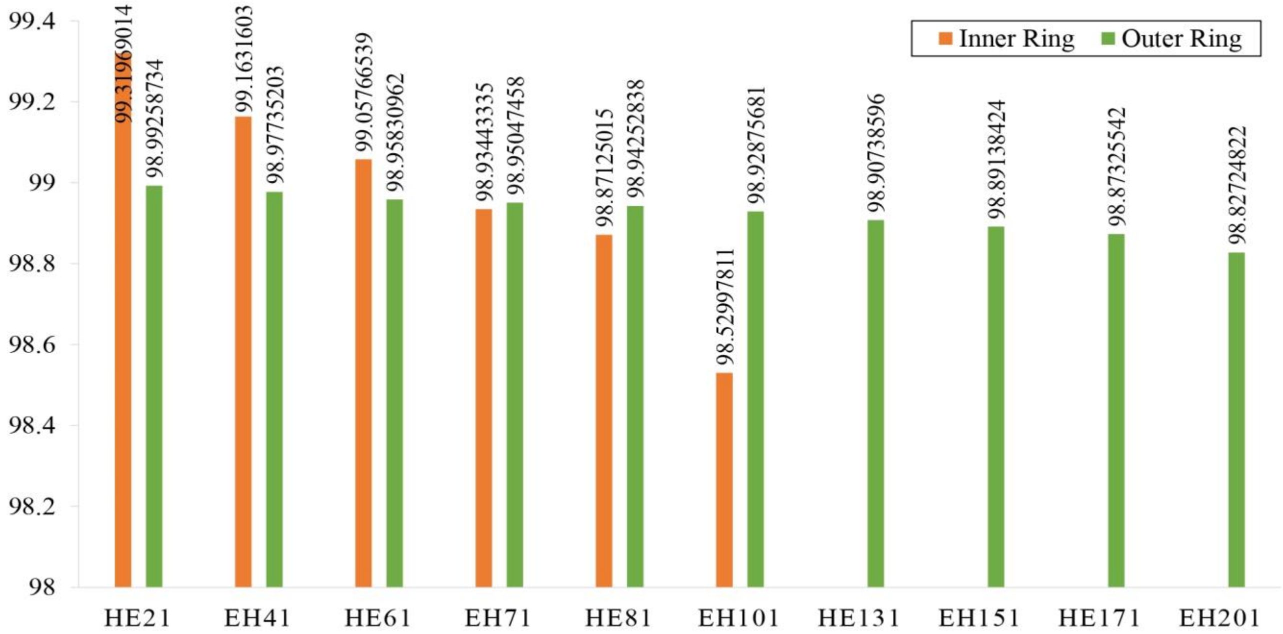

Figure 3.9: Purity assessment of OAM modes at specific states.

The designed nested PCF achieves OAM mode purity exceeding *98%* for both inner and outer rings, with the highest purity observed for the $HE_{2,1}$ mode at *99.31969%* and *98.99258%*, respectively. Thus, plentiful OAM modes, higher OAM purity, and increased intensity greatly boost MDM (Mode Division Multiplex) technology for better OAM mode amplification.

Isolation (ISO) parameters:

Higher isolation parameters positively impact both the effectiveness of isolation and the efficiency of fiber optics transmission. Figure 3.10 (a) and (b) illustrates how the isolation parameter changes across the wavelength range of *0.6* to *1.00* μm. Figure 3.10 also depicts an inverse correlation between wavelength and ISO, indicating that as the wavelength increases, ISO decreases for both inner and outer rings.

(a)

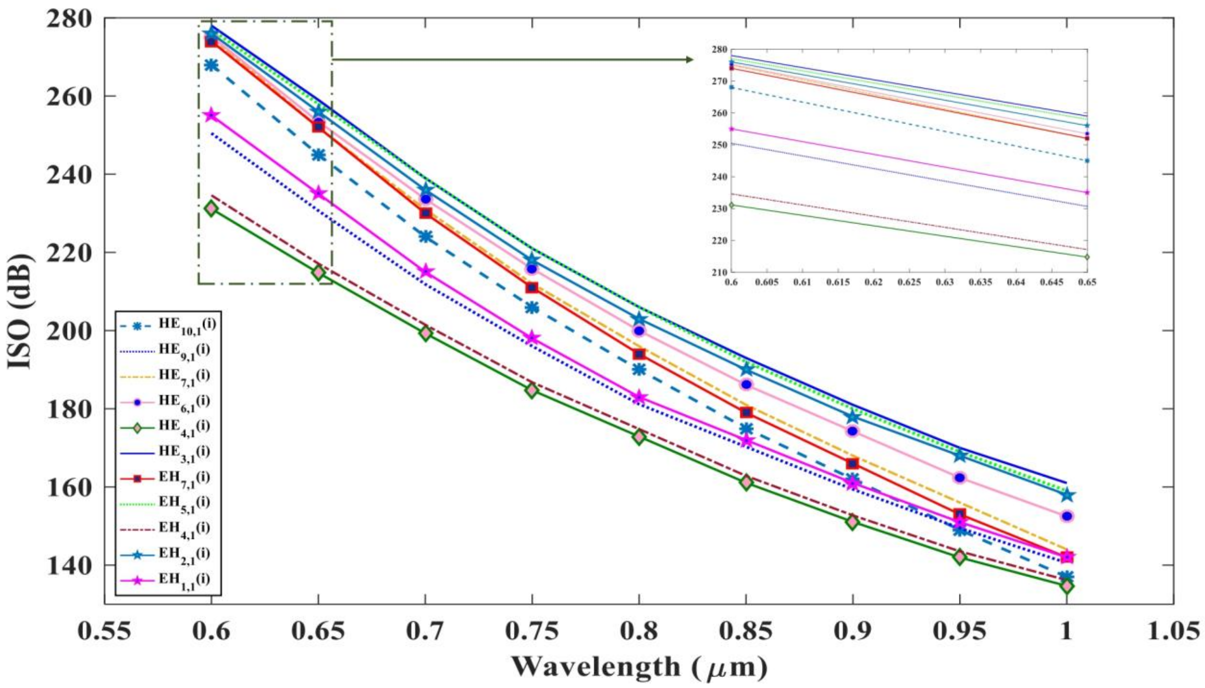

(b)

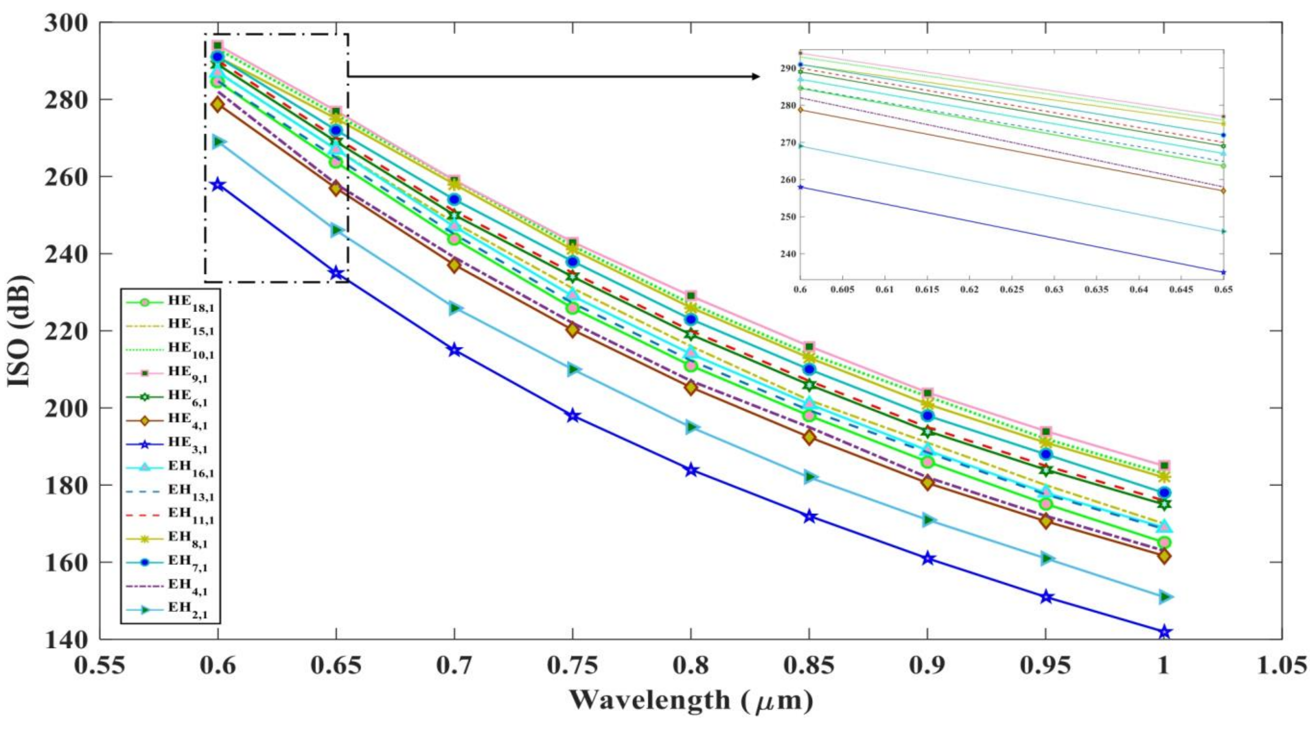

Figure 3.10: ISO of the proposed nested PCF for (a) nodal ring-supported modes, (b) marginal ring-supported modes with respect to wavelength.

Hence, the negligible crosstalk between directed states in the suggested PCF leads to high isolation, ensuring an optical fiber communications system with large capacity.

Chapter 4

Performance Evaluation of the Proposed PCF

4.1 Comparative Analysis

This research introduces a unique architecture for PCF that can accomodate a good quantiyt of optical modalities. The design consists of two sets of rings, with the inner rings having circular air holes and the outer rings having an H-shaped configuration. This design allows the PCF to support $76 + 36$ OAM modes, which are a type of optical mode that has a well-defined orbital angular momentum.

Importantly, the independence of these rings ensures minimal crosstalk between regions associated with different modes, demonstrating a sound ISO value of $294\ dB$. The designed nested PCF is characterized by a significant Effective Refractive Index Difference (ERID), a relatively lower and consistently flat dispersion variation ($-896\ ps/km-nm$), and a large Effective Mode Field Area ($25.8\ \mu m^2$) over a bandwidth of $400\ nm$.

The nested PCF achieves over *98%* OAM mode purity in both nodal and marginal rings, with the $HE_{2,1}$ mode purity reaching *99.31969%* and *98.99258%*, respectively. Numerical findings reveal that the effective refractive index variation among the selected eigenmodes is above 10^{-4}, while simultaneously maintaining a confinement loss below $9.13425 \times 10^{-9}\ dB/m$ across a $400\ nm$ bandwidth. Consequently, the proposed PCF design facilitates increased support for OAM states, a greater effective mode teritorial region alongside reduced anomalous effects. This holds significant importance in ensuring secure and secure and increased data transfer capability in high-speed lightwave interconnections.

In Table 2, a comparative analysis reveals that our proposed PCF surpasses recently published articles in key characteristics, establishing it as an optimal solution for reliable high-speed optics communications.

Table 2: Comparison chart of key atrributes amidst proposed PCF's and Recent Publications

Ref.	Supported Mode	Lowest Confinement Loss (dB/m)	Operating Bandwidth (nm)	Maximum ISO (dB)	Lowest Dispersion Variation $(ps/km-nm)$
[1]	30 + 50	$< 7 \times 10^{-8}$	60	> 40	≤ 2.7
[6]	170 + 62	1.56×10^{-12}	300	> 65	5.9
[7]	64	2.7031×10^{-6}	400	–	-8.838
[8]	38 + 42	1.131×10^{-10}	1200	–	3.7980
[9]	64 + 6	4.05342×10^{-12}	800	126	0.0743
[18]	76 + 6	3.72×10^{-12}	800	171	1.4163
This work	**76 + 36**	$\mathbf{2.49701 \times 10^{-11}}$	**400 nm**	**294 dB**	-856

Overall, this new PCF design has a number of promising features for use in high-speed optical communications. The increased quanity of accomodated OAM states could be employed to increase the potential of transfer capability in high-speed lightwave interconnections. The large effective mode teritorial region could help to reduce nonlinear effects. And the high confinement loss could help to ensure that the signal is not lost as it travels through the fiber.

4.2 Fabrication Possibilities

The designed nested Photonic Crystal Fiber (PCF) structure incorporates a core perforation bordered by two high refractive index rings and cladding. The PCF integrates a dual-layer inner ring with air holes and eight H-shaped circular air holes in the outer ring, streamlining the fabrication process for efficiency and simplicity.

Figure 3.1 clearly depicts the positioning of the inner and outer rings in the cladding region, each featuring 32 and 56 air holes, respectively.

The PCF was constructed utilizing fused silica as the base material, featuring a couple of circular high refractive index shells made of Borosilicate glass (SF_6). SF_6, a commercially available glass from various specialty glass companies, enables fabrication using the "sol-gel" method, as proposed by Li et al. in 2012 [56]. The "sol-gel" technique is widely employed for its exceptional ability to customize patterns of air holes, adjusting spacing and size as needed.

Furthermore, Huang et al. [57] designed a micro-structured ring-based fiber supporting 70 Orbital Angular Momentum (OAM) modes with Schott sulfur difluoride (SF2) and phosphate glass doping, detailing the fabrication process in 2019. Hence, the proposed nested PCF can also be manufactured using the aforementioned methods.

Fabrication process commences with the utilization of the modified chemical vapor deposition (MCVD) [58] process to construct a preform for the annular-oriented PCF. Subsequently, a rotational sonic perforating equipment [58] was employed for creating a spherical core perforation in Schott glass, resulting in the production of a couple of high refractive index ring shells with varying spatial dimensions, along with custom dies. To prevent air hole collapse, precise control of the drawing tower speed is imperative when employing "stack-and-draw" technology for nested dual-guide modes PCF. Ultimately, the preform undergoes heating within a suitable temperature-controlled environment. Therefore, the proposed PCF will be fabricated using the outlined procedures.

Research Overview and Prospective Explorations

6.1 Research Overview

This study introduces an innovative multi-layered PCF featuring a couple of distinct and independent directed mode areas, collectively supporting a total of 112 orbital angular momentum (OAM) modes, comprising 76 + 36 modes. The designed nested PCF is characterized by a prominent core perforation, incorporating a pair of high refractive index shells composed of Borosilicate glass (SF_6), surrounded by a cladding with fused silica as the background material. The findings indicate wherein the suggested PCF exhibits substantial effective refractive index difference (ERID), along with a consistently flat dispersion profile, expansive effective mode field area and minimal confinement loss across the wavelength range of 0.6 to $1\ \mu m$. The confinement loss (CL) ranges approximately between 2.49701×10^{-11} to $9.13425 \times 10^{-9}\ dB/m$, while highest attained OAM purity is *99.31969%* and *98.99258%* at $HE_{2,1}$ mode respectively for both inner and outer rings. All the modes demonstrate ERIDs exceeding 10^{-4} , and minimum dispersion variation observed is $-856\ ps/km - nm$. Additionally, achieving an outstanding isolation performance, with the highest attained ISO reaching $294\ dB$ at $HE_{9,1}$ mode and observed a substantial effective mode area of $9.15\ \mu m^2$ and $25.8\ \mu m^2$ respectively for inner and outer rings. This research leverages COMSOL Multiphysics' finite element method (FEM) and perfectly matched layer (PML) capabilities alongside MATLAB processing to calculate all key attributes of the suggested fiber. Therefore, the suggested Photonic PCF demonstrates promising prospects for extended-range, high-capacity data transmission within optical communications and applications related to OAM sensing.

6.2 Future Work

Employing the robust capabilities of commercial FEM-based simulation tools, specifically COMSOL Multiphysics 4.4 and MATLAB, we conducted a rigorous investigation into the proposed PCF. The practical fabrication of these PCF is slated for implementation in commercial applications. Our future endeavors involve delving into the development of novel PCFs accomodating both OAM and Linearly Polarized (LP) modes, aiming for superior performance. Furthermore, our research extends to the design of PCFs tailored for guiding terahertz (THz) OAM beams.

Bibliography

[1] Hecht, J., 2015. Understanding fiber optics. Jeff Hecht.

[2] Quimby, R.S., 2006. Photonics and lasers: an introduction. John Wiley & Sons.

[3] Wang, W., Sun, C., Wang, N., & Jia, H. (2020, September). A design of nested photonic crystal fiber with low nonlinear and flat dispersion supporting 30+50 OAM modes. *Optics Communications*, *471*, 125823. https://doi.org/10.1016/j.optcom.2020.125823

[4] Guo, S., Wu, F., Albin, S., Tai, H. and Rogowski, R.S., 2004. Loss and dispersion analysis of microstructured fibers by finite-difference method. Optics Express, 12(15), pp.3341-3352.

[5] Steel, M.J. and Osgood, R.M., 2001. Elliptical-hole photonic crystal fibers. Optics Letters, 26(4), pp.229-231.

[6] Russell, P.S.J., 2006. Photonic-crystal fibers. Journal of lightwave technology, 24(12), pp.4729-4749.

[7] Kim, S.E., Kim, B.H., Lee, C.G., Lee, S., Oh, K. and Kee, C.S., 2012. Elliptical defected core photonic crystal fiber with high birefringence and negative flattened dispersion. Optics express, 20(2), pp.1385-1391.

[8] Saitoh, K., Florous, N. and Koshiba, M., 2005. Ultra-flattened chromatic dispersion controllability using a defected-core photonic crystal fiber with low confinement losses. Optics Express, 13(21), pp.8365-8371.

[9] Richardson, D.J., Fini, J.M. and Nelson, L.E., 2013. Space-division multiplexing in optical fibers. Nature photonics, 7(5), pp.354-362.

[10] Li, S., Li, C., Liu, J., Zhu, L., Xu, Z., Zhou, J., Yang, Q. and Wang, J., 2014, September. Multiple orbital angular momentum (OAM) modes (De) multiplexer based on a single complex phase mask. In 2014 The European Conference on Optical Communication (ECOC) (pp. 1-3). IEEE.

[11] Razzak, S.A. and Namihira, Y., 2008. Tailoring dispersion and confinement losses of photonic crystal fibers using hybrid cladding. Journal of Lightwave technology, 26(13), pp.1909-1914.

[12] Wong, G.K.L., Chen, A.Y.H., Ha, S.W., Kruhlak, R.J., Murdoch, S.G., Leonhardt, R., Harvey, J.D. and Joly, N.Y., 2005. Characterization of chromatic dispersion in photonic crystal fibers using scalar modulation instability. Optics Express, 13(21), pp.8662-8670.

[13] Kabir, M. A., Hassan, M. M., Hossain, M. N., Paul, B. K., & Ahmed, K. (2020, July). Design and performance evaluation of photonic crystal fibers supporting orbital angular momentum states in optical transmission. *Optics Communications*, *467*, 125731. https://doi.org/10.1016/j.optcom.2020.125731

[14] Mehedi Hassan, M., Abdulrazak, L. F., Alharbi, A. G., Ahmed, K., Bui, F. M., Al-Zahrani, F. A., & Uddin, M. S. (2022, December). Novel approach of anti-resonant fiber with supporting 64 orbital angular momentum modes for optical communication. *Alexandria Engineering Journal*, *61*(12), 9891–9900. https://doi.org/10.1016/j.aej.2022.03.006

[15] Habib, M.S., Habib, M.S., Hasan, M.I., Razzak, S.M.A., Mahmud, R.R. and Namihira, Y., 2013. Microstructure holey fibers as wideband dispersion compensating media for high speed transmission systems. Optik, 124(21), pp.4984-4988.

[16] Priya, K.R., Raja, A.S. and Sundar, D.S., 2016. Design of a dual-core liquid-filled photonic crystal fiber coupler and analysis of its optical characteristics. Journal of Optical technology, 83(9), pp.569- 573.

[17] Li, S. and Wang, J., 2014. A compact trench-assisted multi-orbital angular-momentum multi-ring fiber for ultrahigh-density space division multiplexing (19 ringsÃU 22 modes). Scientific reports, 4, p.3853.

[18] Mizuno, T., Takara, H., Sano, A. and Miyamoto, Y., 2016. Dense space-division multiplexed transmission systems using multi-core and multi-mode fiber. Journal of lightwave technology, 34(2), pp.582-592.

[19] Igarashi, K., Soma, D., Wakayama, Y., Takeshima, K., Kawaguchi, Y., Yoshikane, N., Tsuritani, T., Morita, I. and Suzuki, M., 2016. Ultradense spatial-division-multiplexed optical fiber transmission over 6-mode 19-core fibers. Optics express, 24(10), pp.10213-10231.

[20] Yu, Y., Lian, Y., Hu, Q., Xie, L., Ding, J., Wang, Y., & Lu, Z. (2022, April 18). Design of PCF Supporting 86 OAM Modes with High Mode Quality and Low Nonlinear Coefficient. *Photonics*, *9*(4), 266. https://doi.org/10.3390/photonics9040266

[21] Willner, A.E., Huang, H., Yan, Y., Ren, Y., Ahmed, N., Xie, G., Bao, C., Li, L., Cao, Y., Zhao, Z. and Wang, J., 2015. Optical communications using orbital angular momentum beams. Advances in Optics and Photonics, 7(1), pp.66-106.

[22] Zhang, L., Zhang, K., Peng, J., Deng, J., Yang, Y. and Ma, J., 2018. Circular photonic crystal fiber supporting 110 OAM modes. Optics Communications, 429, pp.189-193.

[23] Al-Zahrani, F. A., & Mehedi Hassan, M. (2021, December). Enhancement of OAM and LP modes based on double guided ring fiber for high capacity optical communication. *Alexandria Engineering Journal*, *60*(6), 5065–5076. https://doi.org/10.1016/j.aej.2021.04.052

[24] Deng, Y., Zhang, H., Li, H., Tang, X., Xi, L., Zhang, W., & Zhang, X. (2017, February 17). Erbium-doped amplification in circular photonic crystal fiber supporting orbital angular momentum modes. *Applied Optics*, *56*(6), 1748. https://doi.org/10.1364/ao.56.001748

[25] Zhang, H., Zhang, W., Xi, L., Tang, X., Zhang, X. and Zhang, X., 2016. A new type of circular photonic crystal fiber for orbital angular momentum mode transmission. IEEE Photonics Technology Letters, 28(13), pp.1426-1429.

[26] Bozinovic, N., Yue, Y., Ren, Y., Tur, M., Kristensen, P., Huang, H., Willner, A.E. and Ramachandran, S., 2013. Terabit-scale orbital angular momentum mode division multiplexing in fibers. science, 340(6140), pp.1545-1548.

[27] Wang, N., Xie, J.L., Jia, H.Z. and Chen, M.M., 2018. A low confinement loss double-photonic crystal fiber over 850 nm bandwidth with 26 orbital angular momentum modes transmission. Journal of Modern Optics, 65(18), pp.2060-2064.

[28] Allen, L., Beijersbergen, M.W., Spreeuw, R.J.C. and Woerdman, J.P., 1992. Orbital angular momentum of light and the transformation of Laguerre-Gaussian laser modes. Physical review A, 45(11), p.8185

[29] Sueda, K., Miyaji, G., Miyanaga, N. and Nakatsuka, M., 2004. Laguerre-Gaussian beam generated with a multilevel spiral phase plate for high intensity laser pulses. Optics express, 12(15), pp.3548-3553.

[30] Ye, J., Li, Y., Han, Y., Deng, D., Guo, Z., Gao, J., Sun, Q., Liu, Y. and Qu, S., 2016. Excitation and separation of vortex modes in twisted air-core fiber. Optics Express, 24(8), pp.8310-8316.

[31] Zhang, H., Zhang, W., Xi, L., Tang, X., Tian, W., Zhang, X. and Zhang, X., 2015, November. Design of a circular photonic crystal fiber supporting OAM modes. In Asia Communications and Photonics Conference (pp. ASu2A-54). Optical Society of America.

[32] Nandam, A. and Shin, W., 2018. Spiral photonic crystal fiber structure for supporting orbital angular momentum modes. Optik, 169, pp.361-367.

[33] Wan, X., Wang, Z., Sun, B. and Zhang, Z., 2020. Low dispersion and confinement loss photonic crystal fiber for orbital angular momentum mode transmission. Optical and Quantum Electronics, 52(6).

[34] Hu, Z.A., Huang, Y.Q., Luo, A.P., Cui, H., Luo, Z.C. and Xu, W.C., 2016. Photonic crystal fiber for supporting 26 orbital angular momentum modes. Optics express, 24(15), pp.17285-17291.

[35] Xu, X., Jia, H., Lei, Y., Jia, C., Liu, G., Chai, J., Peng, Y. and Xie, J., 2017. Theoretical proposal of a low-loss wide-bandwidth silicon photonic crystal fiber for supporting 30 orbital angular momentum modes. PloS one, 12(12), p.e0189660.

[36] Y. Kang, Y. Shang, F. Pang, N. Chen, Y. Dong, L. Xu, Z. Chen, The OAM transmission fiber based on step-index and graded-index refractive distribution, in: 17th International Conference on Optical Communications and Networks, 2019.

[37] Zhang, H., Zhang, W., Xi, L., Tang, X., Tian, W., Zhang, X., & Zhang, X. (2015). Design of a Circular Photonic Crystal Fiber Supporting OAM Modes. *Asia Communications and Photonics Conference 2015*. https://doi.org/10.1364/acpc.2015.asu2a.54

[38] Jiao, X., Zhang, H., Zhang, X., Li, H., Wei, J., Wang, Z., Xi, L., Zhang, W., & Tang, X. (2019, May 21). Performance of circular photonic crystal fiber transmitting orbital angular momentum modes under macro-bending. *Journal of Optics*, *21*(6), 065703. https://doi.org/10.1088/2040-8986/ab1c44

[39] Li, H., Zhang, H., Zhang, X., Deng, Y., Xi, L., Tang, X., & Zhang, W. (2017, July). Design tools for circular photonic crystal fibers supporting orbital angular momentum modes. *2017 Opto-Electronics and Communications Conference (OECC) and Photonics Global Conference (PGC)*. https://doi.org/10.1109/oecc.2017.8114874

[40] Zhang, H., Zhang, W., Xi, L., Tang, X., Zhang, X., & Zhang, X. (2016, July 1). A New Type Circular Photonic Crystal Fiber for Orbital Angular Momentum Mode Transmission. *IEEE Photonics Technology Letters*, *28*(13), 1426–1429. https://doi.org/10.1109/lpt.2016.2551325

[41] Brunet, C., Vaity, P., Messaddeq, Y., LaRochelle, S., & Rusch, L. A. (2014, October 16). Design, fabrication and validation of an OAM fiber supporting 36 states. *Optics Express*, *22*(21), 26117. https://doi.org/10.1364/oe.22.026117

[42] Xu, M., Zhou, G., Chen, C., Zhou, G., Sheng, Z., Hou, Z., & Xia, C. (2018, August 24). A novel micro-structured fiber for OAM mode and LP mode simultaneous transmission. *Journal of Optics*, *47*(4), 428–436. https://doi.org/10.1007/s12596-018-0487-5

[43] Xu, M., Zhou, G., Chen, C., Zhou, G., Sheng, Z., Hou, Z. and Xia, C., 2018. A novel micro-structured fiber for OAM mode and LP mode simultaneous transmission. Journal of Optics, 47(4), pp.428-436.

[44] Yang, M., Liu, W., Song, Y., Wang, J., Wei, Z., Meng, H., Liu, H., Huang, Z., Xiang, L., Li, H., & Wang, F. (2022, February 4). A design of dual guided modes ring-based photonic crystal fiber supporting 170 + 62 OAM modes with large effective mode field area. *Applied Physics B*, *128*(3). https://doi.org/10.1007/s00340-022-07761-7

[45] Pakarzadeh, H. and Sharif, V., 2019. Control of orbital angular momentum of light in optofluidic infiltrated circular photonic crystal fibers. Optics Communications, 438, pp.18-24.

[46] Hassan, M. M., Kabir, M. A., Hossain, M. N., Biswas, B., Paul, B. K., & Ahmed, K. (2019, November 28). Photonic crystal fiber for robust orbital angular momentum transmission: design and investigation. *Optical and Quantum Electronics*, *52*(1). https://doi.org/10.1007/s11082-019-2125-0

[47] Jia, C., Jia, H., Wang, N., Chai, J., Xu, X., Lei, Y., Liu, G., Peng, Y. and Xie, J., 2018. Theoretical analysis of a 750-nm bandwidth hollow-core ring photonic crystal fiber with a graded structure for transporting 38 orbital angular momentum modes. IEEE Access, 6, pp.20291-20297.

[48] Jia, C., Jia, H., Wang, N., Chai, J., Xu, X., Lei, Y., Liu, G., Peng, Y., & Xie, J. (2018). Theoretical Analysis of a 750-nm Bandwidth Hollow-Core Ring Photonic Crystal Fiber With a Graded Structure for Transporting 38 Orbital Angular Momentum Modes. *IEEE Access*, *6*, 20291–20297. https://doi.org/10.1109/access.2018.2817577

[49] Tian, W., Zhang, H., Zhang, X., Xi, L., Zhang, W., & Tang, X. (2016, July). A circular photonic crystal fiber supporting 26 OAM modes. *Optical Fiber Technology*, *30*, 184–189. https://doi.org/10.1016/j.yofte.2016.07.009

[50] Yue, Y., Yan, Y., Ahmed, N., Yang, J.Y., Zhang, L., Ren, Y., Huang, H., Birnbaum, K.M., Erkmen, B.I., Dolinar, S. and Tur, M., 2012. Mode properties and propagation effects of optical orbital angular momentum (OAM) modes in a ring fiber. IEEE Photonics Journal, 4(2), pp.535-543.

[51] Liu, G., Zhi, Z. and Wang, R.K., 2012. Digital focusing of OCT images based on scalar diffraction theory and information entropy. Biomedical optics express, 3(11), pp.2774-2783.

[52] Hassan, M. M., Kabir, M. A., Hossain, M. N., Nguyen, T. K., Paul, B. K., Ahmed, K., & Dhasarathan, V. (2020, August 7). Numerical analysis of circular core shaped photonic crystal fiber for orbital angular momentum with efficient transmission. *Applied Physics B*, *126*(9). https://doi.org/10.1007/s00340-020-07497-2

[53] White, T.P., McPhedran, R.C., de Sterke, C.M., Botten, L.C. and Steel, M.J., 2001. Confinement losses in microstructured optical fibers. Optics Letters, 26(21), pp.1660-1662.

[54] Xu, M., Zhou, G., Chen, C., Zhou, G., Sheng, Z., Hou, Z. and Xia, C., 2018. A novel micro-structured fiber for OAM mode and LP mode simultaneous transmission. Journal of Optics, 47(4), pp.428-436.

[55] Kabir, M. A., Ahmed, K., Hassan, M. M., Hossain, M. M., & Paul, B. K. (2020, November). Design a photonic crystal fiber of guiding terahertz orbital angular momentum beams in optical communication.*Optics Communications*, *475*, 126192.

https://doi.org/10.1016/j.optcom.2020.126192

[56] El Hamzaoui, H., Ouerdane, Y., Bigot, L., Bouwmans, G., Capoen, B., Boukenter, A., Girard, S., & Bouazaoui, M. (2012, December 20). Sol-gel derived ionic copper-doped microstructured optical fiber: a

potential selective ultraviolet radiation dosimeter. *Optics Express*, *20*(28), 29751. https://doi.org/10.1364/oe.20.029751

[57] Huang, S. H., Ma, Q. C., Chen, W. C., Liu, H. Z., Xing, X. B., Cui, H., Luo, Z. C., Xu, W. C., & Luo, A. P. (2019, October 5). Microstructure ring fiber for supporting higher-order orbital angular momentum modes with flattened dispersion in broad wavebands. *Applied Physics B*, *125*(11). https://doi.org/10.1007/s00340-019-7307-8

[58] X. Feng, A.K. Mairaj, D.W. Hewak, T.M. Monro, Non Silica glasses for holey fibers. J. Lightwave Technol. 23, 2046 (2005)

193-16-464

ORIGINALITY REPORT

12%	5%	11%	2%
SIMILARITY INDEX	INTERNET SOURCES	PUBLICATIONS	STUDENT PAPERS

PRIMARY SOURCES

1	Md. Anowar Kabir, Md. Mehedi Hassan, Md. Nadim Hossain, Bikash Kumar Paul, Kawsar Ahmed. "Design and performance evaluation of photonic crystal fibers of supporting orbital angular momentum states in optical transmission", Optics Communications, 2020 Publication	1%
2	Weicheng Wang, Chunyang Sun, Ning Wang, Hongzhi Jia. "A design of nested photonic crystal fiber with low nonlinear and flat dispersion supporting 30+50 OAM modes", Optics Communications, 2020 Publication	1%
3	Submitted to Mawlana Bhashani Science and Technology University Student Paper	1%
4	link.springer.com Internet Source	1%
5	Fahad Ahmed Al-Zahrani, Md. Mehedi Hassan. "Enhancement of OAM and LP modes based on double guided ring fiber for	1%